

Disentanglement and Generalization Under Correlation Shifts

Christina M. Funke*
University of Tübingen

Paul Vicol*
University of Toronto
Vector Institute

Kuan-Chieh Wang
University of Toronto
Vector Institute

Matthias Kümmerer†
University of Tübingen

Richard Zemel†
University of Toronto
Vector Institute

Matthias Bethge†
University of Tübingen

Abstract

Correlations between factors of variation are prevalent in real-world data. Machine learning algorithms may benefit from exploiting such correlations, as they can increase predictive performance on noisy data. However, often such correlations are not robust (e.g., they may change between domains, datasets, or applications) and we wish to avoid exploiting them. Disentanglement methods aim to learn representations which capture different factors of variation in latent subspaces. A common approach involves minimizing the mutual information between latent subspaces, such that each encodes a single underlying attribute. However, this fails when attributes are correlated. We solve this problem by enforcing independence between subspaces conditioned on the available attributes, which allows us to remove only dependencies that are not due to the correlation structure present in the training data. We achieve this via an adversarial approach to minimize the conditional mutual information (CMI) between subspaces with respect to categorical variables. We first show theoretically that CMI minimization is a good objective for robust disentanglement on linear problems with Gaussian data. We then apply our method on real-world datasets based on MNIST and CelebA, and show that it yields models that are disentangled and robust under correlation shift, including in weakly supervised settings.

1 Introduction

Disentangled representations can be useful for improving fairness [56], interpretability [1], controllable generative modeling [31], and transfer to downstream tasks [84]. In addition, they can improve robustness on out-of-distribution data [34] (e.g., for domain adaptation [37] and domain generalization [9]). Most research on disentanglement has assumed that the underlying factors of variation in the data are *independent* (e.g., that factors are not correlated). However, this assumption is often violated in real-world settings: for example, in domain adaptation, the class distribution often shifts between domains (yielding a correlation between the class and domain); in natural images, there is often a strong correlation between the foreground and background [6], or between multiple foreground objects that tend to co-occur (e.g., a keyboard and monitor) [82, 10]. Importantly, correlated data occurs in areas that affect people’s lives, including in healthcare [15] and fairness applications [60, 21, 56], and correlation shifts in these applications are common (e.g., demographics are likely to differ from one hospital to another).

The goal of disentanglement is to encode data into independent subspaces that preferably match the ground truth generative factors. A common approach (used in ICA, PCA, and VAEs) is to ensure that the latent subspaces share as little information as possible, for example by minimizing the mutual information (MI) between them. However, recently it has been shown that this fails to disentangle correlated factors [81]. Several works have sought to address this by introducing partial supervision [81, 78, 59]. Here, we show that even under *full* supervision, minimizing the MI can fail: it is impossible to encode generative factors into independent subspaces if they are correlated in the training data. To address this, we propose minimizing the MI between subspaces *conditioned* on the correlated attributes.

The goal of this work is to identify and explain the

Preliminary work. * denotes joint first authors. † denotes joint senior authors.

behaviors of different objective functions for correlated and noisy data in a systematic fashion.

Contributions.

- We establish conditional independence as the correct extension of the classically-used statistical independence between latents when disentangling correlated factors of variation.
- We propose to use the *predictive performance under correlation shift* as a measure of disentanglement applicable to settings with correlated factors of variation.
- On a linear regression problem with Gaussian data, we show that minimizing the *conditional* mutual information (CMI) between latent subspaces yields a model robust to test-time correlation shifts, while minimizing the unconditional MI does not.
- We apply CMI minimization to two tasks based on real-world datasets—a multi-object occluded MNIST task and a CelebA-based task—demonstrating that our approach improves performance under correlation shift relative to baselines.
- We show that our approach can also be applied in weakly supervised settings, and show significant gains compared to baselines.

Our code is available [on Github](#).

2 Background & Related Work

ICA/ISA. Disentanglement is related to blind source separation (BSS), as both problems revolve around the question of identifiability. A classic approach to BSS is Independent Component Analysis (ICA) [20, 40, 8, 68], which assumes statistical independence between the source variables [40, 41]. Independent Subspace Analysis (ISA) [36], or multidimensional ICA [13], is a generalization of ICA where each component is a k -dimensional subspace; dimensions within a subspace may have dependencies, while dimensions from different subspaces must be independent.

Correlations Between Features. With roots in ICA, most research on disentanglement focuses on data that was generated by independent factors, including synthetic benchmarks such as dSprites [61], Shapes3D [12], Cars3D [77], SmallNORB [51], or MPI3D [27]. In real-world datasets on the other hand, factors are often correlated [85, 52]. Träuble et al. [81] pointed out the challenges that arise when attempting to learn disentangled representations on correlated data, and performed a large-scale empirical evaluation of the effect of correlations on widely-used VAE-based disentanglement models. They proposed two

approaches to ameliorate the harmful effects of correlations: 1) introducing weak supervision during training, and 2) labeling data post-hoc to “correct” a pre-trained encoder. Our work shows that even under full supervision, correlated attributes are problematic when enforcing independence between latent subspaces. Causally-informed modeling [87] is another approach to learning disentangled representations and extracting invariant features; an example of this is Invariant Risk Minimization (IRM) [3]. To investigate the effect of correlations systematically, it is common to modify existing datasets to induce correlations, for example by subsampling the data, or by generating synthetic datasets with the desired properties [22, 19, 38, 57]. We follow this approach in our experiments.

Unsupervised and Weakly-Supervised Disentanglement. Disentangled representation learning is often studied in the unsupervised setting, where the ground-truth factors of variation are unknown. Widely-used approaches for this include variational autoencoders (VAEs) [48] and their variants (beta-VAE [33], TC-beta-VAE [16], FactorVAE [45], etc.). However, it was shown by Locatello et al. [57] that the assumption of independent source variables (e.g., attributes) is questionable, and thus that *purely unsupervised* disentanglement may not be possible. This spurred interest in *weakly-supervised* methods [78, 59], where weak supervision is provided in the form of partial labels or grouping information [11, 66, 49]. Recently, it was shown that by conditioning the prior on auxiliary information such as class labels or time indexes, VAEs can be made *identifiable* [44], implying that it is possible to learn the true joint distribution and thus recover the true factors of variation. In this paper, we focus on comparing MI and CMI minimization in the fully-supervised setting.

Domain Adaptation/Generalization. We use predictive performance under correlation shift as a measure for the quality of disentanglement. This is closely related to the fields of domain adaptation and generalization, with the difference that we assume access to one source domain only. The goal of most related work in this field is to learn representations from multiple source domains that transfer to known (e.g., adaptation) or previously unseen (e.g., generalization) target domains. This is done by either learning domain-invariant representations which discard domain information [83] or by learning disentangled representations, with latent subspaces that correspond to the domain and the class, respectively [73, 37, 54]. For the latter approach, disentanglement is achieved by minimizing the mutual information between latent subspaces [17, 26, 66]. Zhao et al. [88] discuss fundamental

problems inherent in learning domain-invariant representations when there are correlations between classes and domains (e.g., when the class distribution shifts in the target domain).

Fairness. An important application of disentanglement is fairness. As machine learning systems are typically trained on historical data, they often inherit past biases (e.g., from human decision-makers). This may result in unfair treatment on the basis of sensitive properties such as ethnicity, gender, or disability. Typically, this can be addressed by modifying the training data to be unbiased or by adding a regularizer (e.g. based on mutual information) that quantifies and minimizes the degree of bias [42, 43, 86, 30, 18].

Mutual Information. The mutual information (MI) between two random variables \mathbf{x} and \mathbf{y} , denoted $I(\mathbf{x}; \mathbf{y})$, is the KL divergence between the joint distribution $p(\mathbf{x}, \mathbf{y})$ and the product of the marginal distributions $p(\mathbf{x})p(\mathbf{y})$: $I(\mathbf{x}; \mathbf{y}) = D_{\text{KL}}[p(\mathbf{x}, \mathbf{y}) || p(\mathbf{x})p(\mathbf{y})]$. Many approaches for representation learning are based on maximizing the MI between the data and learned representations [69, 32, 35, 5, 80]; in addition, minimization of MI has been used to implement an information bottleneck [2] and to factorize representations [38]. MI minimization is at the heart of many approaches to disentanglement. The *conditional mutual information* (CMI) is defined as:

$$I(\mathbf{x}; \mathbf{y} | \mathbf{z}) = \mathbb{E}_{\mathbf{z}} [D_{\text{KL}}[p(\mathbf{x}, \mathbf{y} | \mathbf{z}) || p(\mathbf{x} | \mathbf{z})p(\mathbf{y} | \mathbf{z})]]$$

CMI measures the dependency between two variables given that we know the value of a third variable. For example, there is a dependency between a country’s number of Nobel laureates per capita and chocolate consumption per capita [76]. However, this dependency is largely explained by the wealth of a country, thus $I(\text{nobel}; \text{chocolate} | \text{wealth}) < I(\text{nobel}; \text{chocolate})$. In general, the CMI can be smaller or larger than the unconditional MI.

Estimating & Optimizing Mutual Information. Many approaches have been proposed for MI and CMI estimation and optimization. The Mutual Information Neural Estimator (MINE) [7] uses a lower-bound of the MI based on the Donsker-Varadhan dual representation of the KL divergence [23]. Poole et al. [75] provide an overview of variational bounds that can be used to estimate MI; most are *lower bounds*, which are useful in principle for *maximizing* MI, but which have also been used to minimize MI (even though minimizing a lower bound is not guaranteed to decrease MI). CLUB [17] introduced a variational upper bound of MI, providing a more principled objective for minimizing MI. Several CMI estimators have been proposed, including conditional-MINE [62], C-MI-GAN [64], CCMI [65],

and an approach based on nearest neighbors [63]. Many approaches to MI minimization are based on batchwise shuffling of latent subspaces, sometimes referred to as metamer sampling [7, 66, 25, 71, 73]. The approach we use in Section 4 follows this paradigm of latent-space shuffling.

3 Disentangling Correlated Variables

A summary of notation is provided in Appendix A.

Problem Statement. Suppose we observe noisy data $\mathbf{x} \in \mathbb{R}^m$ obtained from an (unknown) generative process $\mathbf{x} = g(\mathbf{s})$ where $\mathbf{s} = (s_1, s_2, \dots, s_K)$ are the *underlying factors of variation*, also called source variables or attributes, which may be correlated with each other. We wish to find a transformation $f: \mathbb{R}^m \rightarrow \mathbb{R}^n$ to a latent space $f(\mathbf{x}) = \mathbf{z} = (\mathbf{z}_1, \mathbf{z}_2, \dots, \mathbf{z}_K)$ such that each of the original attributes s_k can be recovered from the corresponding subspace \mathbf{z}_k by a linear mapping \mathbf{R}_k , e.g., $\hat{s}_k = \mathbf{R}_k \mathbf{z}_k$. We denote by \mathbf{z}_{-i} the set of subspaces $\{\mathbf{z}_1, \dots, \mathbf{z}_{i-1}, \mathbf{z}_{i+1}, \dots, \mathbf{z}_K\}$. We consider three different objectives for learning the latent subspaces: 1) minimizing a supervised loss L (e.g., mean squared error or cross-entropy), $\sum_{i=1}^K L(\hat{s}_i, s_i)$, denoted “*Base*”; 2) minimizing the *unconditional mutual information between subspaces* in addition to the supervised loss, $\sum_i L(\hat{s}_i, s_i) + I(\mathbf{z}_1, \dots, \mathbf{z}_K)$, denoted “*Base+MI*”; and 3) minimizing the *conditional mutual information between subspaces conditioned on observed attributes*, in addition to the supervised loss, $\sum_i L(\hat{s}_i, s_i) + I(\mathbf{z}_i; \mathbf{z}_{-i} | s_i)$ denoted “*Base+CMI*”.

In this section, we introduce a toy disentanglement problem where all quantities of interest can be computed analytically. First, we show that the supervised loss alone does not yield robust disentangled representations, and we discuss why this is problematic. Then, we show that additionally minimizing the unconditional MI forces the model to learn an *even worse solution*. Finally, we show that minimizing the conditional MI yields appropriately disentangled representations that are robust to correlation shift. This analysis motivates CMI as a good objective for achieving robust disentanglement.

3.1 Full Supervision Does Not Yield Disentanglement

Consider a linear generative model with correlated Gaussian source variables \mathbf{s} , given by:

$$\mathbf{x} = \mathbf{A}\mathbf{s} + \mathbf{n} \quad , \quad \mathbf{s} \sim \mathcal{N}(\mathbf{0}, \mathbf{C}_{\mathbf{s}}) \quad , \quad \mathbf{n} \sim \mathcal{N}(\mathbf{0}, \mathbf{C}_{\mathbf{n}})$$

where \mathbf{A} is the mixing matrix and $\mathbf{C}_{\mathbf{s}}$ and $\mathbf{C}_{\mathbf{n}}$ are the covariance matrices for the source and noise variables,

	Base	Base + MI	Base + CMI
Variance Explained, Training (Corr = 0.8)	91.9%	69.8%	90.9%
Variance Explained, Test (Corr = 0)	87.6%	65.0%	90.9%
Regression Matrix M (where $\hat{\mathbf{s}} = M\mathbf{x}$)	$\begin{pmatrix} 0.81 & 0.14 \\ 0.14 & 0.81 \end{pmatrix}$	$\begin{pmatrix} 1.07 & -0.46 \\ -0.46 & 1.07 \end{pmatrix}$	$\begin{pmatrix} 1 & 0 \\ 0 & 1 \end{pmatrix}$

Table 1: Linear regression under correlation shift for each of the objectives *Base*, *Base+MI*, and *Base+CMI*. Here, the observations and predictions are 2D. Performance under correlation shift drops for optimal regression. The optimal solution under the constraint of minimal MI fails to model the in-distribution correlated training data. The solution with minimal *conditional* MI maintains consistent performance under correlation shift. Note that because the generative process is given by $g(\mathbf{s}) = \mathbf{A}\mathbf{s} = \mathbf{I}\mathbf{s}$, the inverse is $\mathbf{A}^{-1} = \mathbf{I}$. In the last row, we see that only Base + CMI recovers this inverse.

respectively. We assume that \mathbf{x} is observed and wish to disentangle the underlying source variables \mathbf{s} ; this corresponds to finding the mapping \mathbf{A}^{-1} that inverts the data generating process. When we have access to the source variables, a natural approach is to minimize a supervised loss to ensure that each subspace contains information about its attribute. The optimal linear regression solution, both in the least squares sense and with respect to maximum likelihood, is given by the posterior mean:

$$\hat{\mathbf{s}}(\mathbf{x}) = \mathbb{E}[\mathbf{s} \mid \mathbf{x}] = \mathbf{C}_{\mathbf{s}\mathbf{x}}\mathbf{C}_{\mathbf{x}}^{-1}\mathbf{x} \quad (1)$$

where $\mathbf{C}_{\mathbf{s}\mathbf{x}}$ and $\mathbf{C}_{\mathbf{x}}$ are the following covariance matrices:

$$\mathbf{C}_{\mathbf{s}\mathbf{x}} = \mathbb{E}[\mathbf{s}(\mathbf{A}\mathbf{s} + \mathbf{n})^\top] = \mathbf{C}_{\mathbf{s}}\mathbf{A}^\top \quad (2)$$

$$\mathbf{C}_{\mathbf{x}} = \mathbf{A}\mathbf{C}_{\mathbf{s}}\mathbf{A}^\top + \mathbf{C}_{\mathbf{n}} \quad (3)$$

The least-squares optimal mapping $\mathbf{C}_{\mathbf{s}\mathbf{x}}\mathbf{C}_{\mathbf{x}}^{-1}\mathbf{x}$ is not equal to the inverse \mathbf{A}^{-1} of the generative model, as it is biased by the correlation structure $\mathbf{C}_{\mathbf{s}}$ and $\mathbf{C}_{\mathbf{n}}$ towards directions of maximal signal-to-noise ratio. Thus, regression is sensitive to noise and does not disentangle the underlying sources. This is problematic, as becomes apparent when computing prediction errors on correlation-shifted data. For this Gaussian problem, we can compute the expected mean squared error (and therefore the expected variance explained) analytically:

$$\mathbb{E}[(\mathbf{s} - \hat{\mathbf{s}}(\mathbf{x}))^2] = \text{Var}(\mathbf{s}) = \text{Tr}(\mathbf{C}_{\mathbf{s}}) \quad (4)$$

In Table 1, we see that in the two-dimensional case where $\mathbf{s} = (s_1, s_2)$ for $\mathbf{A} = \mathbf{I}$, $\sigma = 0.1$ and $\text{corr}(s_1, s_2) = 0.8$, $\hat{\mathbf{s}}$ explains 91.9% of the variance in \mathbf{s} (column “Base”). However, when s_1 and s_2 are uncorrelated, performance drops to 87.6%. This drop occurs because the estimator $\hat{\mathbf{s}}$ tries to make use of the assumed correlation between s_1 and s_2 to counteract the information lost due to noise, but this correlation is no longer present in the test data. The gap in performance between correlated and uncorrelated data indicates that s_1 and s_2 have not been correctly disentangled.

3.2 Unconditional Disentanglement Fails Under Correlation Shift

In the 2D linear case, we have:

$$\mathbf{z} = (z_1, z_2) = \mathbf{W}\mathbf{x}, \quad \hat{s}_1 = R_1 z_1, \quad \hat{s}_2 = R_2 z_2 \quad (5)$$

where the matrix \mathbf{W} encodes the observation into the latent space. The linear regression example in Sec. 3.1 corresponds to $\mathbf{W} = \mathbf{C}_{\mathbf{s}\mathbf{x}}\mathbf{C}_{\mathbf{x}}^{-1}$ and $R_k = 1$. In standard supervised objectives, there is no constraint preventing a subspace z_k from containing information about other source variables than s_k . A common approach to counter the lack of generalization is to minimize the MI between the latent subspaces z_1 and z_2 [16, 73]. In the Gaussian case, random variables are independent if and only if they are *decorrelated*. The optimal linear regression weights that yield $I(z_1; z_2) = 0$ (e.g., \mathbf{W} such that $\text{Cov}(\mathbf{z})$ is diagonal) can be computed by whitening \mathbf{x} and rotating the result by an angle ϕ_{opt} which leads to maximal VE ($\phi_{\text{opt}} = -\pi/4$ for positive correlations and $\mathbf{A} = \mathbf{I}$). See Figure 7 in Appendix B for details. However, the resulting model no longer performs well on in-distribution-data (Table 1, column “Base+MI”). There is correlation between the sources s_1 and s_2 and therefore $I(s_1; s_2) > 0$. By enforcing independence, at least one of the subspaces cannot contain all relevant information about its target value and therefore will have poor predictive performance. We make this precise in the following proposition.

Proposition 3.1. *If $I(s_1; s_2) > 0$, then enforcing $I(z_1; z_2) = 0$ leads to $I(z_k; s_k) < H(s_k)$ for at least one k .*

Proof. We provide the proof in Appendix D. \square

3.3 Conditional Disentanglement is Robust to Correlation Shift

We have seen that enforcing unconditional independence between the latent spaces does not solve the disentanglement problem. However, from the graphical model (Appendix B, Fig. 6), it is clear that \mathbf{z}_1 and

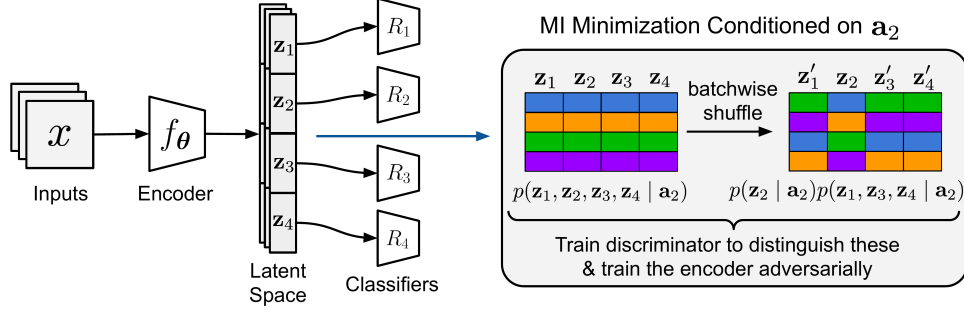


Figure 1: **Adversarial minimization of conditional mutual information via latent-space shuffling.** We minimize the CMI between latent subspaces, $I(\mathbf{z}_1; \dots; \mathbf{z}_K | \mathbf{a}_k)$. Here, we illustrate the algorithm for four attributes with corresponding latent spaces $\{\mathbf{z}_1, \mathbf{z}_2, \mathbf{z}_3, \mathbf{z}_4\}$, where we condition on attribute \mathbf{a}_2 .

Algorithm 1 Learning Conditionally Disentangled Subspaces Adversarially — Training the Encoder

```

1: Input:  $\{\phi_1, \dots, \phi_K\}$ , initial parameters for  $K$  linear classifiers  $R_1, \dots, R_K$ 
2: Input:  $\theta$ , initial parameters for the encoder  $f$ 
3: Input:  $\alpha, \beta$  learning rates for training the encoder and linear classifiers
4: while true do
5:    $(\mathbf{x}, \{\mathbf{a}_k\}_{k=1}^K) \sim \mathcal{D}_{\text{Train}}$                                 ▷ Sample a minibatch of data with attribute labels
6:    $\mathbf{z} \leftarrow f_{\theta}(\mathbf{x})$                                           ▷ Forward pass through the encoder
7:    $\{\mathbf{z}_k\}_{k=1}^K \leftarrow \text{SplitSubspaces}(\mathbf{z}, K)$                 ▷ Partition the latent space into  $K$  subspaces
8:    $L \leftarrow \sum_{k=1}^K L_{\text{cls}}(R_k(\mathbf{z}_k; \phi_k), \mathbf{a}_k)$           ▷ Cross-entropy for each attribute
9:   for  $k \in \{1, \dots, K\}$  do                                     ▷ For each attribute/subspace
10:     $\mathbf{z}' \sim p(\mathbf{z}_1, \dots, \mathbf{z}_K | \mathbf{a}_k)$                         ▷ Samples from the joint distribution
11:     $\mathbf{z}'' \sim p(\mathbf{z}_k | \mathbf{a}_k)p(\mathbf{z}_{-k} | \mathbf{a}_k)$                   ▷ Samples w/ batchwise-shuffled subspaces
12:     $L \leftarrow L + \log(1 - D_{\omega}(\mathbf{z}'')) + \log(D_{\omega}(\mathbf{z}'))$     ▷ Add adversarial loss
13:   end for
14:    $\theta \leftarrow \theta - \alpha \nabla_{\theta} L$                                 ▷ Update encoder parameters
15:    $\phi_k \leftarrow \phi_k - \beta \nabla_{\phi_k} L$  ,  $\forall k \in \{1, \dots, K\}$   ▷ Update classifier parameters
16: end while
    
```

\mathbf{z}_2 are independent *conditioned on either of s_1 or s_2* . Assuming a common cause for the correlation between s_1 and s_2 , there is a connection in the graphical model between \mathbf{z}_1 and \mathbf{z}_2 introducing the statistical dependence. Observing either s_1 or s_2 disconnects \mathbf{z}_1 and \mathbf{z}_2 . Here, we show that enforcing independence *conditioned on each of the source variables* is also sufficient to yield a robust disentangled representation. For our 2D example, enforcing conditional independence corresponds to:

$$I(\mathbf{z}_1; \mathbf{z}_2 | s_1) = 0 \quad \text{and} \quad I(\mathbf{z}_1; \mathbf{z}_2 | s_2) = 0 \quad (6)$$

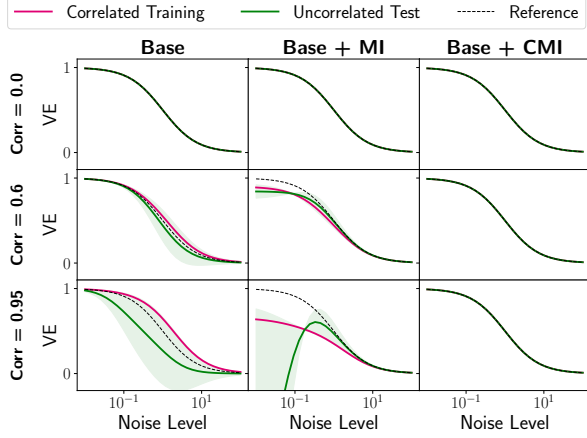
Intuitively, if s_1 and s_2 are correlated, then $I(s_1; s_2) > 0$ and knowing s_1 gives us information about s_2 . If we can predict s_1 from \mathbf{z}_1 , and s_1 tells us about s_2 , then it must be the case that \mathbf{z}_1 contains information about s_2 . We wish to ensure that \mathbf{z}_1 and \mathbf{z}_2 share as little information as possible (given the ground-truth correlation), to improve robustness to shifts. Since \mathbf{z}_1 necessarily contains some information about s_2 , we enforce that it does not contain *any more information about \mathbf{z}_2 than necessary* via $I(\mathbf{z}_1, \mathbf{z}_2 | s_2)$, which states

that if we know s_2 , then knowing \mathbf{z}_1 does not give us more information about \mathbf{z}_2 .

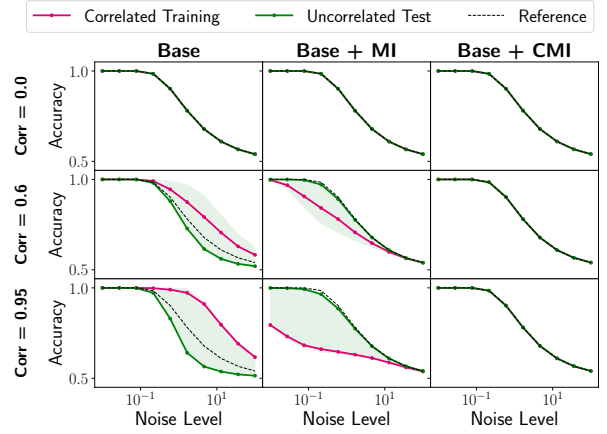
This does not penalize \mathbf{z}_1 for containing information about s_2 due to correctly predicting the correlated variable s_1 (and vice versa). In contrast to MI, this removes only the shared information which is not robust under correlation shift, but keeps the shared information which is necessary to account for the correlation between the sources. The optimal solution under the constraint of conditional independence is achieved by the mapping $\mathbf{W} = \mathbf{A}^{-1}$, successfully recovering the underlying generative model. This demonstrates the usefulness of minimizing CMI for generalization under correlation shifts in the case of linear regression with Gaussian variables where all quantities are analytically tractable, and motivates us to investigate CMI minimization for larger-scale tasks.

4 Minimizing CMI

We formally describe the algorithms for the baselines (*Base* and *Base + MI*) in Appendix C.



(a) Toy linear regression.



(b) Toy classification with ten attributes.

Figure 2: Synthetic linear regression and linear classification tasks. We investigate the impact of the correlation strength and noise level when using each of the objectives *Base*, *Base+MI*, and *Base+CMI*. We measure the variance explained for regression and accuracy for classification. We compare the objectives (columns) with different training correlations (rows). In both tasks, we sweep over noise levels in the range $[10^{-2}, 10^2]$. The base models in the uncorrelated setting serve as a reference (dashed black line). **Magenta:** performance on correlated training data. **Green:** performance on test data with a range of correlation shifts (solid line: uncorrelated data; shaded region: correlations in the range $[-1, 1]$ for regression, and only positive correlations for classification). In both regression and classification tasks, we find that *Base+CMI* leads to robustness under correlation shift, while the other approaches do not.

In simple cases such as linear regression, we can compute and minimize the MI/CMI analytically; however, for most tasks (including classification), there is no closed form for the mutual information. In this section, we describe our approach to minimize the CMI in general classification settings.

Suppose we have a dataset $\mathcal{D} = \{(\mathbf{x}^{(i)}, \mathbf{a}^{(i)})\}_{i=1}^N$ where $\mathbf{x}^{(i)}$ is an example and $\mathbf{a}^{(i)}$ is a vector of attribute labels— $\mathbf{a}_k^{(i)}$ is the label for the k^{th} attribute of the i^{th} example. We consider discrete attribute values, $\mathbf{a}_k^{(i)} \in \mathbb{N}$. Let $f_{\theta} : \mathbf{x} \mapsto \mathbf{z}$ denote an encoder function parameterized by θ that maps examples $\mathbf{x} \in \mathbb{R}^m$ to latent representations $\mathbf{z} \in \mathbb{R}^n$. We aim to learn one latent subspace per attribute, such that each subspace is independent from all other subspaces conditioned on the encoded attribute. Note that the dimensions m and n are arbitrary—in particular, n does not need to be smaller than m . In principle, each subspace can have different dimension (e.g., the linear readout layer for each attribute can have arbitrary dimensions $A \times S$ where A is the attribute dimensionality and S is the dimensionality of a particular subspace).

$I(\mathbf{x}; \mathbf{y} | \mathbf{z}) = 0$ if $p(\mathbf{x}, \mathbf{y} | \mathbf{z}) = p(\mathbf{x} | \mathbf{z})p(\mathbf{y} | \mathbf{z})$. Our method enforces this condition using an adversarial discriminator. To obtain samples from $p(\mathbf{z}_1, \dots, \mathbf{z}_K | \mathbf{a}_k)$ and $p(\mathbf{z}_k | \mathbf{a}_k)p(\mathbf{z}_{-k} | \mathbf{a}_k)$, we loop over values of \mathbf{a}_k , and for each condition $\{\mathbf{a}_k = 0, \mathbf{a}_k = 1, \dots\}$, we select examples from the minibatch that satisfy the condition,

giving us samples from $p(\mathbf{z}_1, \dots, \mathbf{z}_K | \mathbf{a}_k)$; then we shuffle the latent subspaces $\mathbf{z}_j, \forall j \neq k$ jointly batchwise (e.g., combining \mathbf{z}_k from one example with \mathbf{z}_{-k} from another) to obtain samples from $p(\mathbf{z}_k | \mathbf{a}_k)p(\mathbf{z}_{-k} | \mathbf{a}_k)$. To enforce $p(\mathbf{z}_1, \dots, \mathbf{z}_K | \mathbf{a}_k) = p(\mathbf{z}_k | \mathbf{a}_k)p(\mathbf{z}_{-k} | \mathbf{a}_k)$, we train the encoder f adversarially against a discriminator trained to distinguish between these two distributions. The discriminator takes as input a representation and predicts whether it is “real” (e.g., drawn from the joint distribution) or “fake” (e.g., drawn from the product of marginals). One discriminator is trained for each attribute \mathbf{a}_k , which receives samples from the two distributions and the attribute value it is conditioned on. In practice, we use a conditional discriminator, effectively sharing parameters between the discriminators for each of the attributes. This process is illustrated in Figure 1. Algorithm 1 describes the encoder training loop; Algorithm 5 in Appendix C describes the corresponding discriminator training loop.

This approach is architecture-agnostic, and can be used to factorize the latent space of any classifier or generative model (e.g., VAEs [39] or flow-based models [47]). However, note that different models (e.g., VAEs) may have objectives that interfere with the goal of obtaining conditionally independent subspaces (for example, the ELBO encourages independence between all latent dimensions). We chose not to use VAEs to avoid this conflicting objective, and instead consider simple linear and MLP encoders.

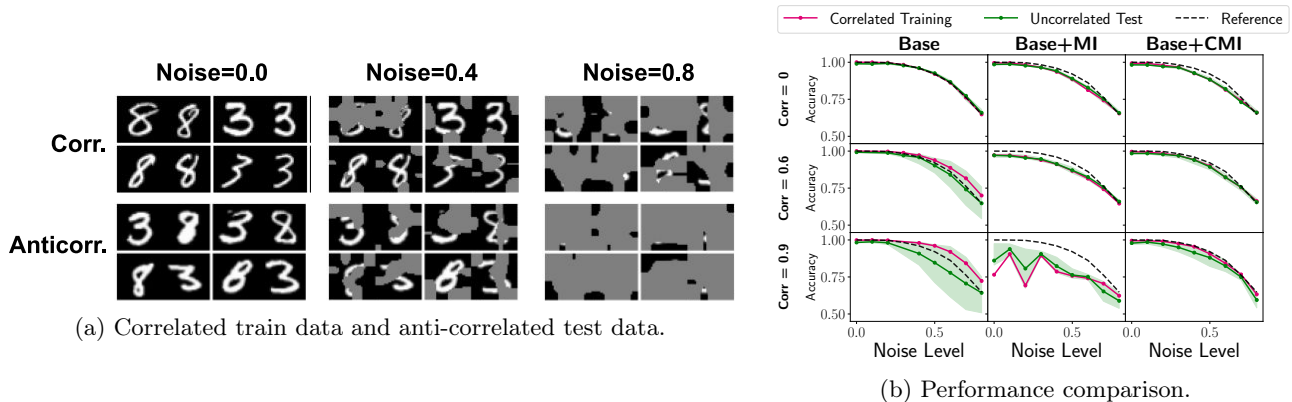


Figure 3: **Multi-digit occluded MNIST.** (a) Occlusions are generated for each of the left and right digits separately. We visualize both correlated training data (where 3-3 and 8-8 pairs are frequent) and anticorrelated test data (where 3-8 and 8-3 pairs are frequent), under a range of occlusion strengths. (b) Accuracies under correlation shifts for different noise levels, achieved by training with each of the objective functions *Base*, *Base+MI*, and *Base+CMI*.

Note that because the latent space is typically low-dimensional, we have a choice of different distribution alignment techniques, including maximum mean discrepancy (MMD) [29] and adversarial approaches [28]. Different GAN formulations can be interpreted as minimizing different divergences: the vanilla GAN formulation [28] minimizes the Jensen-Shannon divergence; WGAN [4] minimizes the Wasserstein distance, which has been used to define an analogue of mutual information called the *Wasserstein dependency measure* [70]; *f*-GAN [67] minimizes an arbitrary *f*-divergence, etc. Note that all these divergence measures are 0 if and only if the subspaces in question are independent, however the behavior of each divergence may differ during training. In practice, we found the vanilla GAN formulation to work well across our experiments.

5 Experiments

First, we present results on the analytically-solvable linear regression example, illustrating the effect of the correlation strength and noise level on the solution obtained by each objective. Then, we employ the method described in Section 4 and demonstrate that our findings also hold for a toy classification task with multiple attributes. Next, we investigate two realistic tasks, namely a multi-digit MNIST task with occlusions and a correlated version of CelebA, and show that minimizing CMI can largely eliminate the gap in performance under correlation shift. Finally, we evaluate common disentanglement metrics and apply our approach in weakly supervised settings. In general, the attributes can take on arbitrary categorical values; for our experiments we use binary attributes for simplicity. Experimental details and extended results are provided in Appendix B.

Toy Linear Regression. In the linear regression problem in Section 3, we evaluated the performance under correlation shift for one specific noise level and correlation strength. In this experiment we varied these parameters and found that our findings hold over all noise levels and non-zero correlation strengths. As shown in Figure 2a, the performance of *Base* drops most severely under correlation shift for strong correlations and intermediate noise levels. In this regime, the advantage of *Base+CMI* shows most clearly. Additional results and intuitive explanations can be found in Appendix B.1.

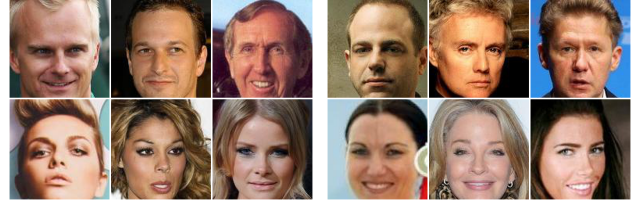
Toy Multi-Attribute Classification. The purpose of this experiment is to test in a controlled setting if our findings hold for classification tasks with multiple attributes. Here, the binary source attributes $a_k = \pm 1, \forall k \in \{1, \dots, K\}$ generate the observed data via $\mathbf{x} = \mathbf{A}\mathbf{a} + \mathbf{n}$ (we set $\mathbf{A} = \mathbf{I}$ for simplicity) with normally distributed noise $\mathbf{n} \sim \mathcal{N}(\mathbf{0}, \mathbf{C}_n)$. We induce correlations between the attributes a_k , such that the number of datapoints differs for the different combinations of attribute values. In the multi-attribute setting, the correlation strength refers to the pairwise correlation between all attributes. As for the regression task, we find that *Base+CMI* leads to robustness under correlation shift (Figure 2b and Appendix B.2).

Multi-Digit Occluded MNIST. Next, we designed a larger-scale task to investigate whether these properties hold in a more complex setting. We created a dataset by concatenating two MNIST digits side-by-side, where the aim is to predict both the left- and right-hand-side labels. We used a subset of MNIST consisting of classes 3 and 8 (which are visually similar and can become ambiguous under occlusions). We generated occlusion masks using the procedure from [14];

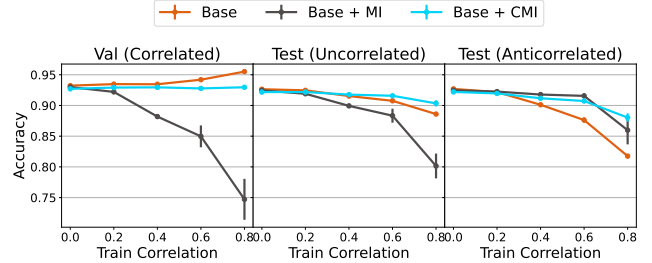
examples from our synthetic dataset under a range of noise settings are shown in Figure 3a. This mimics the multiple-object classification setting in a way that allows us to control the correlation strength and noise level (via the amount of occlusion), allowing for systematic analysis. While this would also be possible for colored MNIST and dSprites, one advantage of our choice is the symmetry of our task, which allows us to exclude potential side-effects: here, the attributes have the same type (the digit identity), whereas the attributes in colored MNIST (digit identity and color) and dSprites (shape, size, position, etc.) are more diverse.

Similarly to the toy tasks, we train an encoder to map images onto a D -dimensional latent space, which is partitioned in two equal-sized subspaces corresponding to the two digits; we train a linear classifier on each subspace to predict the respective class labels. We consider different correlation strengths between the left and right digits in the training set (where strong correlation means that the digits match most of the time, e.g., 3-3 or 8-8 are more common than 3-8 or 8-3). We evaluate each model on test data with correlation strengths ranging from $[-1, 1]$. The results are shown in Figure 3b. We found that the conclusions from the toy experiments hold in this setting: supervised learning with only the classification loss, as well as with unconditional MI minimization, fails under test-time correlation shift, while the model minimizing conditional MI is more robust. Additional details are provided in Appendix B.3.

CelebA. Finally, we consider a realistic setting using the CelebA [55] faces dataset. In contrast to the multi-digit MNIST case, here we do not add any artificial observation noise. We considered two attributes that we know *a priori* are not causally related, **Male** and **Smiling**, and we created subsampled datasets that satisfied specific correlations between attributes. We investigated a range of training correlations $\{0, 0.2, 0.4, 0.6, 0.8\}$, and evaluated our models on both *anti-correlated* and *uncorrelated* test sets (Figures 4a and 4b). Figure 4c compares the performance of the baseline classifier, unconditional MI model, and conditionally disentangled model under a range of correlation strengths. We found that minimizing CMI has a larger effect for medium-to-high correlation; however, CMI minimization does not hurt performance at low correlation strengths. Note that while the unconditional model appears to have good performance on the anti-correlated test set, its performance is poor on the validation set (that has the same correlation structure as the training set), so this model does not perform well on in-distribution-data. In contrast, the conditional MI model performs well on both in-distribution-data and



(a) Correlated train data. (b) Anti-correlated test data.



(c) Performance comparison.

Figure 4: **Correlated CelebA.** (a) Training examples with correlation 0.8 between attributes **Male** and **Smiling**, such that the majority of men are smiling while the majority of women are not. (b) Anti-correlated test examples, where the majority of women are smiling. (c) Accuracies of each method under a range of correlation strengths, for validation data with the same correlation as the training data, uncorrelated test data, and anticorrelated test data.

shifted test distributions. Also note that the problem of disentangling correlated attributes does not occur only under correlation shift, but is already present in the source domain where certain attribute combinations will reliably be treated incorrectly. For example, *Base* fails to recognize the rare non-smiling male faces in 49% of the cases, while *Base+CMI* fails only in 25% of the cases. Additional details are in Appendix B.4.

Disentanglement Metrics. Previous work [58] has shown that common disentanglement metrics are not suitable for the correlated setting. For this reason, we focused on comparing performance under correlation shift, which we consider more suitable for correlated data: if a model cannot predict a factor of variation well for certain values of another factor, then the model did not successfully disentangle these factors of variation. However, one can still make use of the disentanglement metrics by evaluating them on *uncorrelated* data using the models trained on correlated data. We performed this analysis for toy classification and for CelebA, and found that *Base+CMI* leads to better disentanglement scores across a range of metrics, compared to the other objectives (Appendix B.5).

Extension to Weakly Supervised Settings. Our method can be applied directly to weakly supervised

settings. Importantly, it is not necessary to have labels for multiple attributes for a single data point. We find that when reducing the number of labels, *Base+CMI* outperforms the other objectives under correlation shift (Figure 5 and Appendix B.6).

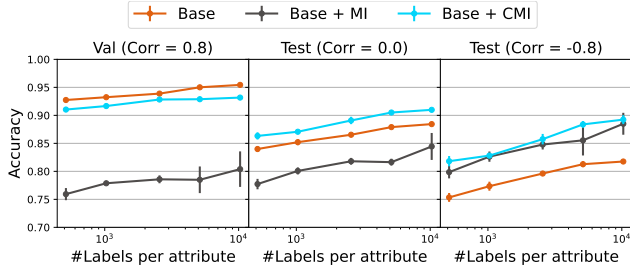


Figure 5: **Weakly-supervised CelebA.** The x-axis shows the number of labels per attribute used during training; the rightmost datapoint corresponds to full supervision. Here, *Base+CMI* outperforms the other objectives under correlation shift.

6 Limitations & Future Work

Our approach requires access to attribute labels in order to shuffle latent subspaces appropriately, and thus is only applicable to categorical attributes. Minimizing CMI yields predictions that disregard correlations between attributes in the training data; we have shown that this is helpful when correlations shift between the training and test data. However, some correlations may reflect the true structure of the world (e.g., they are unlikely to shift between training and test data) and in such cases, ignoring correlations may harm performance. A direction for future work would be to automatically determine which correlations are more or less likely to shift in held-out data.

Estimating the conditional MI requires batchwise shuffling of latent subspaces for each attribute that is being conditioned on. The cost of computing CMI scales linearly with the number of attributes and attribute values, while the cost of computing the unconditional MI is constant, because it does not require restricted sampling/shuffling of latents.

7 Conclusion

Correlations are prevalent in real-world data, yet pose a substantial challenge for disentangled representation learning. Standard approaches learn to rely on these correlations, and when the attributes are not causally related, this leads to poor performance under test-time correlation shift. Although for small correlations the effects may not be large, relying on these correlations and thereby treating a few datapoints systematically incorrectly, can be catastrophic for fairness. We first showed that supervised learning and *unconditional* mutual in-

formation minimization, fail to learn representations robust to such shifts. We then argued that the correct notion of disentanglement in such cases is *conditional disentanglement*, and we proposed a simple approach to minimize the conditional mutual information between latent subspaces. We showed that conditionally disentangled representations improve robustness to correlation shift in toy linear tasks, as well as on natural images. Overall, we established CMI minimization as a more appropriate alternative to MI minimization, which sets the stage for the development of more powerful objective functions for disentanglement.

Acknowledgements

We thank Jörn-Henrik Jacobsen for his valuable contributions in the early stage of this work. We thank Steffen Schneider, Dylan Paiton, Lukas Schott, Elliot Creager, and Frederik Träuble for helpful discussions. We thank the International Max Planck Research School for Intelligent Systems (IMPRS-IS) for supporting Christina Funke. Paul Vicol was supported by a JP Morgan AI Fellowship.

We acknowledge support from the German Federal Ministry of Education and Research (BMBF) through the Competence Center for Machine Learning (FKZ 01IS18039A) and the Bernstein Computational Neuroscience Program Tübingen (FKZ: 01GQ1002), the German Excellence Initiative through the Centre for Integrative Neuroscience Tübingen (EXC307), and the Deutsche Forschungsgemeinschaft (DFG; Projektnummer 276693517 – SFB 1233). Resources used in preparing this research were provided, in part, by the Province of Ontario, the Government of Canada through CIFAR, and companies sponsoring the Vector Institute www.vectorinstitute.ai/partners.

References

- [1] Tameem Adel, Zoubin Ghahramani, and Adrian Weller. Discovering interpretable representations for both deep generative and discriminative models. In *International Conference on Machine Learning (ICML)*, pages 50–59, 2018.
- [2] Alexander A Alemi, Ian Fischer, Joshua V Dillon, and Kevin Murphy. Deep variational information bottleneck. *arXiv preprint arXiv:1612.00410*, 2016.
- [3] Martin Arjovsky, Léon Bottou, Ishaan Gulrajani, and David Lopez-Paz. Invariant risk minimization. *arXiv preprint arXiv:1907.02893*, 2019.
- [4] Martin Arjovsky, Soumith Chintala, and Léon Bottou. Wasserstein generative adversarial networks. In *International Conference on Machine Learning (ICML)*, pages 214–223, 2017.
- [5] Philip Bachman, R Devon Hjelm, and William Buchwalter. Learning representations by maximizing

- mutual information across views. *arXiv preprint arXiv:1906.00910*, 2019.
- [6] Sara Beery, Grant Van Horn, and Pietro Perona. Recognition in terra incognita. In *European Conference on Computer Vision (ECCV)*, pages 456–473, 2018.
- [7] Mohamed Ishmael Belghazi, Aristide Baratin, Sai Rajeswar, Sherjil Ozair, Yoshua Bengio, Aaron Courville, and R Devon Hjelm. MINE: Mutual information neural estimation. In *International Conference on Machine Learning (ICML)*, 2018.
- [8] Anthony J Bell and Terrence J Sejnowski. The “independent components” of natural scenes are edge filters. *Vision Research*, 37(23):3327–3338, 1997.
- [9] Aharon Ben-Tal, Laurent El Ghaoui, and Arkadi Nemirovski. *Robust Optimization*. Princeton University Press, 2009.
- [10] Lucas Beyer, Olivier J Hénaff, Alexander Kolesnikov, Xiaohua Zhai, and Aaron van den Oord. Are we done with Imagenet? *arXiv preprint arXiv:2006.07159*, 2020.
- [11] Diane Bouchacourt, Ryota Tomioka, and Sebastian Nowozin. Multi-level variational autoencoder: Learning disentangled representations from grouped observations. In *Proceedings of the AAAI Conference on Artificial Intelligence*, 2018.
- [12] Chris Burgess and Hyunjik Kim. 3D Shapes Dataset. <https://github.com/deepmind/3dshapes-dataset/>, 2018.
- [13] J-F Cardoso. Multidimensional independent component analysis. In *International Conference on Acoustics, Speech and Signal Processing (ICASSP)*, volume 4, pages 1941–1944, 1998.
- [14] Lucy Chai, Jonas Wulff, and Phillip Isola. Using latent space regression to analyze and leverage compositionality in GANs. *arXiv preprint arXiv:2103.10426*, 2021.
- [15] Agisilaos Chartsias, Thomas Joyce, Giorgos Papanastasiou, Scott Semple, Michelle Williams, David Newby, Rohan Dharmakumar, and Sotirios A Tsaftaris. Factorised spatial representation learning: Application in semi-supervised myocardial segmentation. In *International Conference on Medical Image Computing and Computer-Assisted Intervention*, pages 490–498, 2018.
- [16] Ricky TQ Chen, Xuechen Li, Roger B Grosse, and David K Duvenaud. Isolating sources of disentanglement in variational autoencoders. In *Advances in Neural Information Processing Systems (NeurIPS)*, pages 2610–2620, 2018.
- [17] Pengyu Cheng, Weituo Hao, Shuyang Dai, Jiachang Liu, Zhe Gan, and Lawrence Carin. Club: A contrastive log-ratio upper bound of mutual information. In *International Conference on Machine Learning (ICML)*, pages 1779–1788, 2020.
- [18] Jaewoong Cho, Gyeongjo Hwang, and Changho Suh. A fair classifier using mutual information. In *International Symposium on Information Theory (ISIT)*, pages 2521–2526. IEEE, 2020.
- [19] Mircea Cimpoi, Subhransu Maji, Iasonas Kokkinos, Sammy Mohamed, and Andrea Vedaldi. Describing textures in the wild. In *Conference on Computer Vision and Pattern Recognition (CVPR)*, pages 3606–3613, 2014.
- [20] Pierre Comon. Independent component analysis, a new concept? *Signal Processing*, 36(3):287–314, 1994.
- [21] Elliot Creager, David Madras, Jörn-Henrik Jacobsen, Marissa A Weis, Kevin Swersky, Toniann Pitassi, and Richard Zemel. Flexibly fair representation learning by disentanglement. *arXiv preprint arXiv:1906.02589*, 2019.
- [22] Andrea Dittadi, Frederik Träuble, Francesco Locatello, Manuel Wüthrich, Vaibhav Agrawal, Ole Winther, Stefan Bauer, and Bernhard Schölkopf. On the transfer of disentangled representations in realistic settings. *arXiv preprint arXiv:2010.14407*, 2020.
- [23] Monroe D Donsker and SR Srinivasa Varadhan. Asymptotic evaluation of certain Markov process expectations for large time. *Communications on Pure and Applied Mathematics*, 36(2):183–212, 1983.
- [24] Cian Eastwood and Christopher KI Williams. A framework for the quantitative evaluation of disentangled representations. In *International Conference on Learning Representations (ICLR)*, 2018.
- [25] Zunlei Feng, Xinchao Wang, Chenglong Ke, An-Xiang Zeng, Dacheng Tao, and Mingli Song. Dual swap disentangling. In *Advances in Neural Information Processing Systems (NeurIPS)*, pages 5894–5904, 2018.
- [26] Behnam Gholami, Pritish Sahu, Ognjen Rudovic, Konstantinos Bousmalis, and Vladimir Pavlovic. Unsupervised multi-target domain adaptation: An information theoretic approach. *IEEE Transactions on Image Processing*, 29:3993–4002, 2020.
- [27] Muhammad Waleed Gondal, Manuel Wüthrich, Đorđe Miladinović, Francesco Locatello, Martin Breidt, Valentin Volchkov, Joel Akpo, Olivier Bachem, Bernhard Schölkopf, and Stefan Bauer. On the transfer of inductive bias from simulation to the real world: A new disentanglement dataset. *arXiv preprint arXiv:1906.03292*, 2019.
- [28] Ian J Goodfellow, Jean Pouget-Abadie, Mehdi Mirza, Bing Xu, David Warde-Farley, Sherjil Ozair, Aaron Courville, and Yoshua Bengio. Generative adversarial networks. *arXiv preprint arXiv:1406.2661*, 2014.
- [29] Arthur Gretton, Karsten Borgwardt, Malte Rasch, Bernhard Schölkopf, and Alex Smola. A kernel method for the two-sample problem. *Advances in Neural Information Processing Systems (NeurIPS)*, 19:513–520, 2006.
- [30] Moritz Hardt, Eric Price, and Nathan Srebro. Equality of opportunity in supervised learning. *arXiv preprint arXiv:1610.02413*, 2016.
- [31] Zhenliang He, Wangmeng Zuo, Meina Kan, Shiguang Shan, and Xilin Chen. AttGAN: Facial attribute editing by only changing what you want. *IEEE Transactions on Image Processing*, 28(11):5464–5478, 2019.

- [32] Olivier J Hénaff, Ali Razavi, Carl Doersch, SM Eslami, and Aaron van den Oord. Data-efficient image recognition with contrastive predictive coding. *arXiv preprint arXiv:1905.09272*, 2019.
- [33] Irina Higgins, Loic Matthey, Arka Pal, Christopher Burgess, Xavier Glorot, Matthew Botvinick, Shakir Mohamed, and Alexander Lerchner. Beta-VAE: Learning basic visual concepts with a constrained variational framework. In *International Conference on Learning Representations (ICLR)*, 2017.
- [34] Irina Higgins, Arka Pal, Andrei A Rusu, Loic Matthey, Christopher P Burgess, Alexander Pritzel, Matthew Botvinick, Charles Blundell, and Alexander Lerchner. DARLA: Improving zero-shot transfer in reinforcement learning. *arXiv preprint arXiv:1707.08475*, 2017.
- [35] R Devon Hjelm, Alex Fedorov, Samuel Lavoie-Marchildon, Karan Grewal, Adam Trischler, and Yoshua Bengio. Learning deep representations by mutual information estimation and maximization. *arXiv preprint arXiv:1808.06670*, 2018.
- [36] Aapo Hyvärinen and Patrik Hoyer. Emergence of phase-and shift-invariant features by decomposition of natural images into independent feature subspaces. *Neural Computation*, 12(7):1705–1720, 2000.
- [37] Maximilian Ilse, Jakub M Tomczak, Christos Louizos, and Max Welling. DIVA: Domain invariant variational autoencoders. In *Medical Imaging with Deep Learning*, pages 322–348, 2020.
- [38] Jörn-Henrik Jacobsen, Jens Behrmann, Richard Zemel, and Matthias Bethge. Excessive invariance causes adversarial vulnerability. *arXiv preprint arXiv:1811.00401*, 2018.
- [39] Tom Joy, Sebastian Schmon, Philip Torr, N Siddharth, and Tom Rainforth. Capturing label characteristics in VAEs. In *International Conference on Learning Representations (ICLR)*, 2020.
- [40] Christian Jutten and Jeanny Herault. Blind separation of sources, part I: An adaptive algorithm based on neuromimetic architecture. *Signal Processing*, 24(1):1–10, 1991.
- [41] Christian Jutten and Juha Karhunen. Advances in nonlinear blind source separation. In *International Symposium on Independent Component Analysis and Blind Signal Separation (ICA2003)*, pages 245–256, 2003.
- [42] Faisal Kamiran and Toon Calders. Classifying without discriminating. In *2nd International Conference on Computer, Control and Communication*, pages 1–6. IEEE, 2009.
- [43] Toshihiro Kamishima, Shotaro Akaho, and Jun Sakuma. Fairness-aware learning through regularization approach. In *11th International Conference on Data Mining Workshops*, pages 643–650. IEEE, 2011.
- [44] Ilyes Khemakhem, Diederik Kingma, Ricardo Monti, and Aapo Hyvärinen. Variational autoencoders and nonlinear ICA: A unifying framework. In *International Conference on Artificial Intelligence and Statistics (AISTATS)*, pages 2207–2217, 2020.
- [45] Hyunjik Kim and Andriy Mnih. Disentangling by factorising. In *International Conference on Machine Learning (ICML)*, pages 2649–2658, 2018.
- [46] Diederik P Kingma and Jimmy Ba. Adam: A method for stochastic optimization. *arXiv preprint arXiv:1412.6980*, 2014.
- [47] Diederik P Kingma and Prafulla Dhariwal. Glow: Generative flow with invertible 1x1 convolutions. *arXiv preprint arXiv:1807.03039*, 2018.
- [48] Diederik P Kingma and Max Welling. Auto-encoding variational Bayes. *arXiv preprint arXiv:1312.6114*, 2013.
- [49] David Klindt, Lukas Schott, Yash Sharma, Ivan Ustyuzhaninov, Wieland Brendel, Matthias Bethge, and Dylan Paiton. Towards nonlinear disentanglement in natural data with temporal sparse coding. *arXiv preprint arXiv:2007.10930*, 2020.
- [50] Abhishek Kumar, Prasanna Sattigeri, and Avinash Balakrishnan. Variational inference of disentangled latent concepts from unlabeled observations. *arXiv preprint arXiv:1711.00848*, 2017.
- [51] Yann LeCun, Fu Jie Huang, and Leon Bottou. Learning methods for generic object recognition with invariance to pose and lighting. In *Conference on Computer Vision and Pattern Recognition (CVPR)*, volume 2, pages 11–104, 2004.
- [52] Tsung-Yi Lin, Michael Maire, Serge Belongie, James Hays, Pietro Perona, Deva Ramanan, Piotr Dollár, and C Lawrence Zitnick. Microsoft COCO: Common objects in context. In *European Conference on Computer Vision (ECCV)*, pages 740–755, 2014.
- [53] Zinan Lin, Ashish Khetan, Giulia Fanti, and Sewoong Oh. PacGAN: The power of two samples in generative adversarial networks. *Advances in Neural Information Processing Systems (NeurIPS)*, 2018.
- [54] Alexander H Liu, Yen-Cheng Liu, Yu-Ying Yeh, and Yu-Chiang Frank Wang. A unified feature disentangler for multi-domain image translation and manipulation. *arXiv preprint arXiv:1809.01361*, 2018.
- [55] Ziwei Liu, Ping Luo, Xiaogang Wang, and Xiaoou Tang. Deep learning face attributes in the wild. In *International Conference on Computer Vision (ICCV)*, 2015.
- [56] Francesco Locatello, Gabriele Abbati, Thomas Rainforth, Stefan Bauer, Bernhard Schölkopf, and Olivier Bachem. On the fairness of disentangled representations. In *Advances in Neural Information Processing Systems (NeurIPS)*, pages 14611–14624, 2019.
- [57] Francesco Locatello, Stefan Bauer, Mario Lucic, Gunnar Raetsch, Sylvain Gelly, Bernhard Schölkopf, and Olivier Bachem. Challenging common assumptions in the unsupervised learning of disentangled representations. In *International Conference on Machine Learning (ICML)*, pages 4114–4124, 2019.

- [58] Francesco Locatello, Stefan Bauer, Mario Lucic, Gunnar Rätsch, Sylvain Gelly, Bernhard Schölkopf, and Olivier Bachem. A sober look at the unsupervised learning of disentangled representations and their evaluation. *Journal of Machine Learning Research*, 21:1–62, 2020.
- [59] Francesco Locatello, Ben Poole, Gunnar Rätsch, Bernhard Schölkopf, Olivier Bachem, and Michael Tschanen. Weakly-supervised disentanglement without compromises. In *International Conference on Machine Learning (ICML)*, 2020.
- [60] David Madras, Elliot Creager, Toniann Pitassi, and Richard Zemel. Learning adversarially fair and transferable representations. *arXiv preprint arXiv:1802.06309*, 2018.
- [61] Loic Matthey, Irina Higgins, Demis Hassabis, and Alexander Lerchner. dSprites: Disentanglement testing Sprites dataset. <https://github.com/deepmind/dsprites-dataset/>, 2017.
- [62] Sina Molavipour, Germán Bassi, and Mikael Skoglund. Conditional mutual information neural estimator. In *International Conference on Acoustics, Speech and Signal Processing (ICASSP)*, pages 5025–5029, 2020.
- [63] Sina Molavipour, Germán Bassi, and Mikael Skoglund. On neural estimators for conditional mutual information using nearest neighbors sampling. *arXiv preprint arXiv:2006.07225*, 2020.
- [64] Arnab Kumar Mondal, Arnab Bhattacharya, Sudipto Mukherjee, Sreeram Kannan, Himanshu Asnani, and Prathosh AP. C-MI-GAN: Estimation of conditional mutual information using MinMax formulation. *arXiv preprint arXiv:2005.08226*, 2020.
- [65] Sudipto Mukherjee, Himanshu Asnani, and Sreeram Kannan. CCM: Classifier based conditional mutual information estimation. In *Uncertainty in Artificial Intelligence*, pages 1083–1093, 2020.
- [66] Jozsef Nemeth. Adversarial disentanglement with grouped observations. In *34th AAAI Conference on Artificial Intelligence*, 2020.
- [67] Sebastian Nowozin, Botond Cseke, and Ryota Tomioka. F-GAN: Training generative neural samplers using variational divergence minimization. *arXiv preprint arXiv:1606.00709*, 2016.
- [68] Bruno A Olshausen and David J Field. Emergence of simple-cell receptive field properties by learning a sparse code for natural images. *Nature*, 381(6583):607–609, 1996.
- [69] Aaron van den Oord, Yazhe Li, and Oriol Vinyals. Representation learning with contrastive predictive coding. *arXiv preprint arXiv:1807.03748*, 2018.
- [70] Sherjil Ozair, Corey Lynch, Yoshua Bengio, Aaron van den Oord, Sergey Levine, and Pierre Sermanet. Wasserstein dependency measure for representation learning. *arXiv preprint arXiv:1903.11780*, 2019.
- [71] Taesung Park, Jun-Yan Zhu, Oliver Wang, Jingwan Lu, Eli Shechtman, Alexei A Efros, and Richard Zhang. Swapping autoencoder for deep image manipulation. In *Advances on Neural Information Processing Systems (NeurIPS)*, 2020.
- [72] Adam Paszke, Sam Gross, Francisco Massa, Adam Lerer, James Bradbury, Gregory Chanan, Trevor Killeen, Zeming Lin, Natalia Gimelshein, Luca Antiga, et al. Pytorch: An imperative style, high-performance deep learning library. *arXiv preprint arXiv:1912.01703*, 2019.
- [73] Xingchao Peng, Zijun Huang, Ximeng Sun, and Kate Saenko. Domain agnostic learning with disentangled representations. In *International Conference on Machine Learning (ICML)*, 2019.
- [74] Ken Perlin. Improving noise. In *29th Annual Conference on Computer Graphics and Interactive Techniques*, pages 681–682, 2002.
- [75] Ben Poole, Sherjil Ozair, Aaron van den Oord, Alexander A Alemi, and George Tucker. On variational bounds of mutual information. *arXiv preprint arXiv:1905.06922*, 2019.
- [76] Aloys Leo Prinz. Chocolate consumption and Nobel laureates. *Social Sciences & Humanities Open*, 2(1):100082, 2020.
- [77] Scott E Reed, Yi Zhang, Yuting Zhang, and Honglak Lee. Deep visual analogy-making. *Advances in Neural Information Processing Systems (NeurIPS)*, 28:1252–1260, 2015.
- [78] Rui Shu, Yining Chen, Abhishek Kumar, Stefano Ermon, and Ben Poole. Weakly supervised disentanglement with guarantees. *arXiv preprint arXiv:1910.09772*, 2019.
- [79] Raphael Suter, Djordje Miladinovic, Bernhard Schölkopf, and Stefan Bauer. Robustly disentangled causal mechanisms: Validating deep representations for interventional robustness. In *International Conference on Machine Learning (ICML)*, pages 6056–6065, 2019.
- [80] Yonglong Tian, Dilip Krishnan, and Phillip Isola. Contrastive multiview coding. *arXiv preprint arXiv:1906.05849*, 2019.
- [81] Frederik Träuble, Elliot Creager, Niki Kilbertus, Anirudh Goyal, Francesco Locatello, Bernhard Schölkopf, and Stefan Bauer. Is independence all you need? On the generalization of representations learned from correlated data. *arXiv preprint arXiv:2006.07886*, 2020.
- [82] Dimitris Tsipras, Shibani Santurkar, Logan Engstrom, Andrew Ilyas, and Aleksander Madry. From Imagenet to image classification: Contextualizing progress on benchmarks. In *International Conference on Machine Learning (ICML)*, pages 9625–9635, 2020.
- [83] Eric Tzeng, Judy Hoffman, Kate Saenko, and Trevor Darrell. Adversarial discriminative domain adaptation. In *Conference on Computer Vision and Pattern Recognition (CVPR)*, pages 7167–7176, 2017.

- [84] Sjoerd Van Steenkiste, Francesco Locatello, Jürgen Schmidhuber, and Olivier Bachem. Are disentangled representations helpful for abstract visual reasoning? In *Advances in Neural Information Processing Systems (NeurIPS)*, pages 14245–14258, 2019.
- [85] P. Welinder, S. Branson, T. Mita, C. Wah, F. Schroff, S. Belongie, and P. Perona. Caltech-UCSD Birds 200. Technical Report CNS-TR-2010-001, California Institute of Technology, 2010.
- [86] Rich Zemel, Yu Wu, Kevin Swersky, Toni Pitassi, and Cynthia Dwork. Learning fair representations. In *International Conference on Machine Learning (ICML)*, pages 325–333, 2013.
- [87] Cheng Zhang, Kun Zhang, and Yingzhen Li. A causal view on robustness of neural networks. *arXiv preprint arXiv:2005.01095*, 2020.
- [88] Han Zhao, Remi Tachet des Combes, Kun Zhang, and Geoffrey J Gordon. On learning invariant representation for domain adaptation. *arXiv preprint arXiv:1901.09453*, 2019.

Appendix

This appendix is structured as follows:

- In Section A we provide an overview of the notation we use throughout the paper.
- In Section B we provide experimental details, as well as extended results.
- In Section C we provide the algorithms for the baseline methods, namely for classification-only training and unconditional mutual information minimization.
- In Section D we provide a proof of Proposition 3.1.

A Notation

Symbol	Meaning
\mathbf{z}	Latent representation
\mathbf{x}	Observations
\mathbf{s}	Ground-truth latent factors
$\hat{\mathbf{s}}$	Factor predictions
\mathbf{W}	Linear regression weights
R_1, R_2	Linear readout from the latent space \mathbf{z} to predictions $\hat{\mathbf{s}}$
ϵ	Isotropic Gaussian noise, $\epsilon \sim \mathcal{N}(0, \sigma^2 I)$
\mathbf{A}	Square matrix used to generate observations for the linear task as $\mathbf{x} = \mathbf{A}\mathbf{s} + \epsilon$
F	Encoder function
\mathbf{a}_k	Label for attribute k

Table 2: Summary of the notation used in this paper.

B Experimental Details and Extended Results

Graphical Model. In Figure 6 we provide the graphical model discussed in Section 3.3.

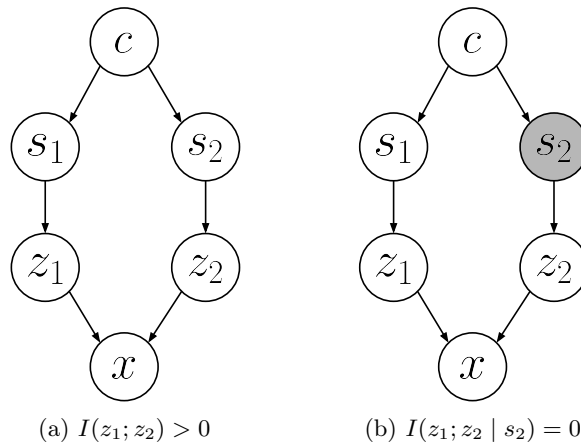


Figure 6: The graphical model for two sources s_1, s_2 and corresponding latent subspaces z_1, z_2 . We assume the source variables have a common cause c . In (a), when none of the sources are observed, there is a path from z_1 to z_2 , so we have $I(z_1; z_2) > 0$; in (b) we observe s_2 , which breaks the path, and thus $I(z_1; z_2 | s_2) = 0$.

Compute Environment. Our experiments were implemented using PyTorch [72], and were run on our internal clusters. The toy 2D experiments were run on a single NVIDIA RTX 2080 TI GPU, and took approximately 48

hours for all the results presented. The MNIST and CelebA experiments were run on NVIDIA Titan Xp GPUs. Each run of the multi-digit MNIST and CelebA tasks for a given method and correlation strength (and noise level in the MNIST case) took approximately 12 hours, and these were run in parallel.

B.1 Toy Linear Regression

Optimal Solution for the Base + MI Objective. Optimal linear regression with zero mutual information between z_1 and z_2 can be obtained by taking the singular value decomposition of \mathbf{x} followed by whitening and rotation by -45° (see Figure 7).

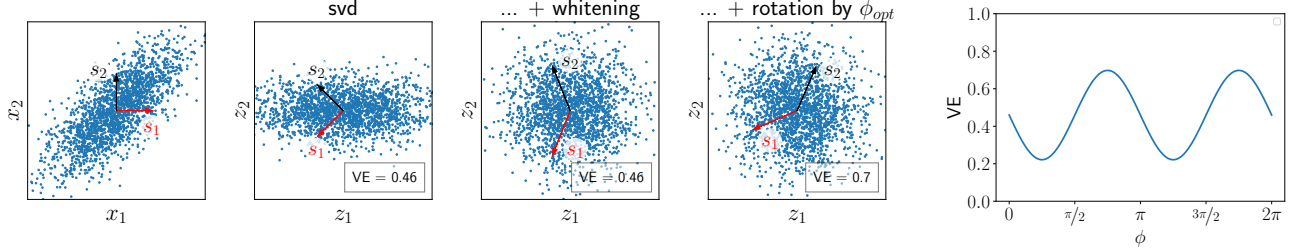


Figure 7: To enforce unconditional independence, we choose \mathbf{W} such that $\text{Cov}(\mathbf{z})$ is diagonal. In our case this is easy: the principal components of \mathbf{x} are $x_1 + x_2$ and $x_1 - x_2$. The optimal regression loss with minimal MI is then given by whitening and rotating the result by angle ϕ_{opt} which leads to maximal VE ($\phi_{\text{opt}} = -\pi/4$ for positive correlations and $\mathbf{A} = \mathbf{I}$).

Intuitive Explanations of the Behavior of the Different Objectives. Comparing the correlation of target \mathbf{s} and data \mathbf{x} with the correlation of the predictions $\hat{\mathbf{s}}$ of the different models can help us understand the findings of Section 3. As shown in Figure 8, the predictions of optimal linear regression (*Base+MI*) ($\text{corr}(\hat{s}_1, \hat{s}_2) = 0.85$) are stronger correlated than the data ($\text{corr}(x_1, x_2) = 0.73$). This shows that the correlation present in the training data is used to compensate for the noise. Enforcing unconditional independence (*Base+MI*) on the other hand, leads to uncorrelated predictions ($\text{corr}(\hat{s}_1, \hat{s}_2) = 0$). Undoubtedly, this cannot be the correct solution, as the targets are correlated. Additionally, when the correlations change, the independence constraint does not hold anymore. This can lead to interesting effects under correlation shift. While for most noise levels, the performance on the test data is poor, for some noise levels the performance can be even higher than training performance (Figure 2a). In these cases the model can "accidentally" exploit the correlation in the test data to make the correct predictions. The correlation of the predictions ($\text{corr}(\hat{s}_1, \hat{s}_2) = 0.73$) matches the correlation of the data only for *Base+CMI*.

B.2 Toy Multi-Attribute Classification

We performed this experiment with two, four and ten binary attributes. The results for varying numbers of attributes are shown in Figure 10. For two attributes we illustrated the data \mathbf{x} for different correlation strength and noise levels (Figure 9). Here, increasing the correlation strength means that data points with $a_1 = a_2$ are increasingly more common relative to $a_1 \neq a_2$. The noise level on the other hand determines the overlap of the distributions and therefore the difficulty of the task.

Experimental Details. We used a PacGAN-style setup [53] for our toy experiments, where the discriminator takes as input a concatenation of 50 samples.

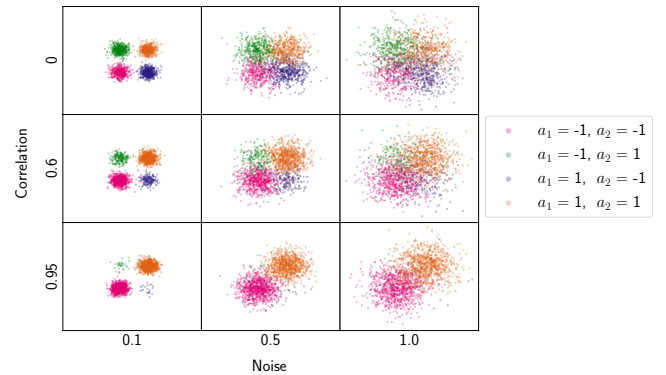


Figure 9: Data used for linear classification with two attributes (a_1 and a_2), visualized for a range of correlation strengths and noise levels.

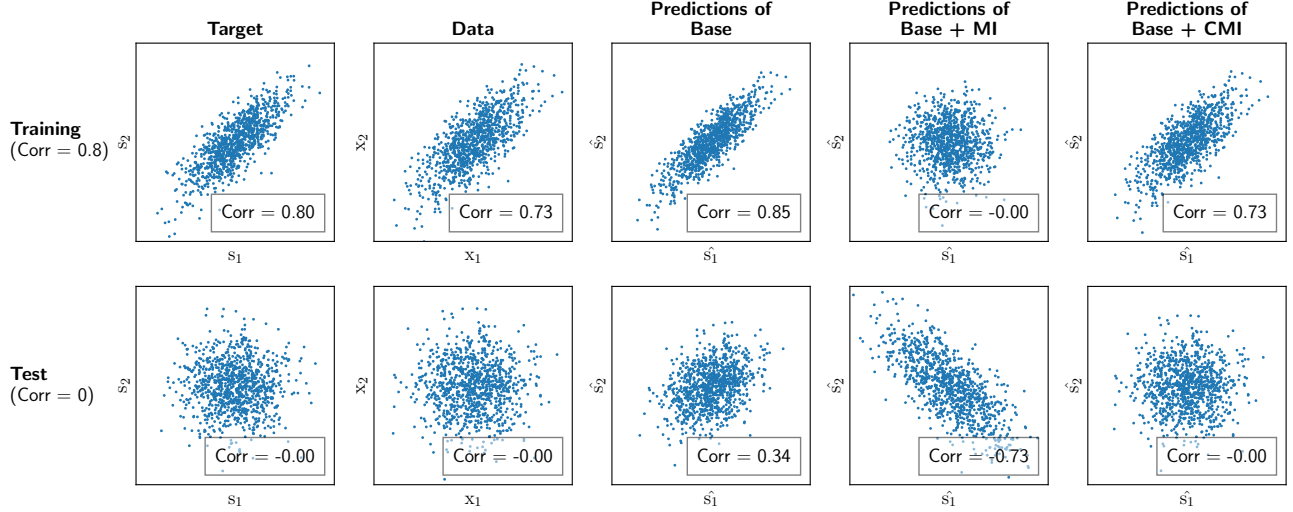


Figure 8: Correlation of target \mathbf{s} , data \mathbf{x} and predictions $\hat{\mathbf{s}}$. Only for conditional independence does the correlation between the predictions and data match for both training and test data. The same setup as for Table 1 was used (two attributes s_1 and s_2 , $\text{corr}(s_1, s_2) = 0.8$, $\mathbf{A} = \mathbf{I}$, $\sigma = 0.1$).

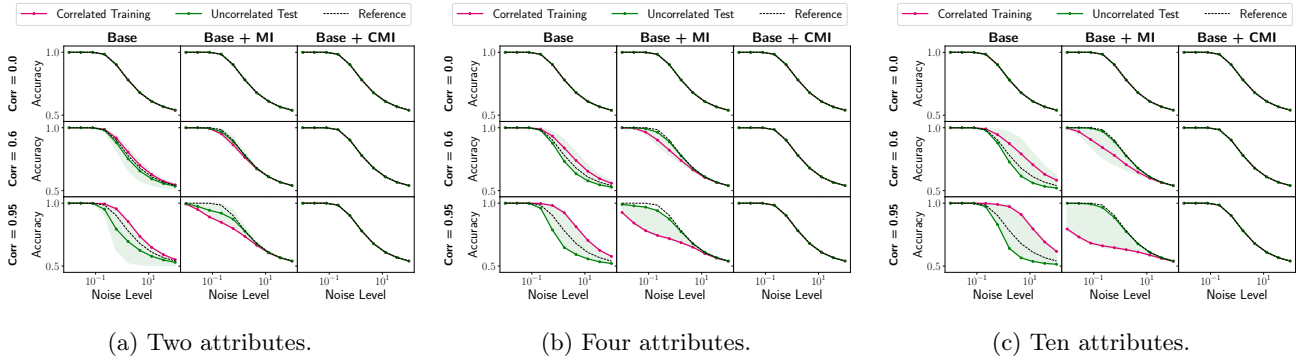


Figure 10: Toy classification with different numbers of attributes. Strong negative correlations could not be generated for multiple attributes; thus only positive test correlations were evaluated for (b) and (c).

- **Base:** We used Adam [46] with a learning rate of 0.01.
- **Base + MI:** We used Adam to optimize the encoder, linear classifiers, and discriminators. After each step of optimizing the discriminator and encoder, we optimized the linear classifiers (R) for 10 steps. The disentanglement loss term was weighted by a factor of 100 relative to the classification loss. In preliminary tests, we found that the optimal learning rate depended on noise level, correlation strength, and number of attributes. The results in Figure 2b were obtained using one of the following learning rates for the discriminator $\{1e-4, 2e-4, 5e-4, 1e-3, 5e-3\}$. The learning rate of the generator and linear classifiers was chosen to be 10 times smaller than the discriminator learning rate.
- **Base + CMI:** For $\mathbf{A} = \mathbf{I}$, no optimization was necessary, as we already know the optimal solution to be $\mathbf{W} = \mathbf{A}^{-1} = \mathbf{I}$. We confirmed experimentally that the discriminator could not get above chance performance for this solution.

B.3 Multi-Object Occluded MNIST

We used minibatch size 100, and latent dimension $D = 10$, yielding two subspaces each of dimension 5. As the encoder model, we used a three-layer MLP with 50 hidden units per layer and ReLU activations. We trained for 400 epochs, using Adam [46] to optimize the encoder, linear classifiers, and discriminators, with separate learning rates for each component chosen via a grid search over $\{1e-5, 1e-4, 1e-3\}$.

Correlated Data Generation. We used the default MNIST training and test splits, and held out 10k of the original training examples to form a validation set, yielding 50k, 10k, and 10k examples in the training, validation, and test sets, respectively. Each digit is first rescaled to be 32×32 pixels. The correlated data was generated on-the-fly during training. Each example in a minibatch was created by: 1) sampling the left-right digit combination (e.g., $\{3-3, 3-8, 8-3, 8-8\}$) from a joint distribution encoding the desired correlation; 2) choosing random instances of each of the selected classes (e.g., a random image of a 3 and a random image of an 8); 3) applying occlusions separately to each image; and 4) concatenating the images, yielding a 32×64 example. This procedure was performed for each training and test minibatch, yielding a larger amount of data than would be possible with a fixed dataset generated *a priori*. To generate occlusions, we use the approach from [14], which produces contiguous masks similar to Perlin noise [74]. We used gray occlusions to remove a potential ambiguity that exists with black masks (which blend into the MNIST background): a masked 8 can become identical to a 3, so one could not tell whether the image is a noisy 8 or a clean 3.

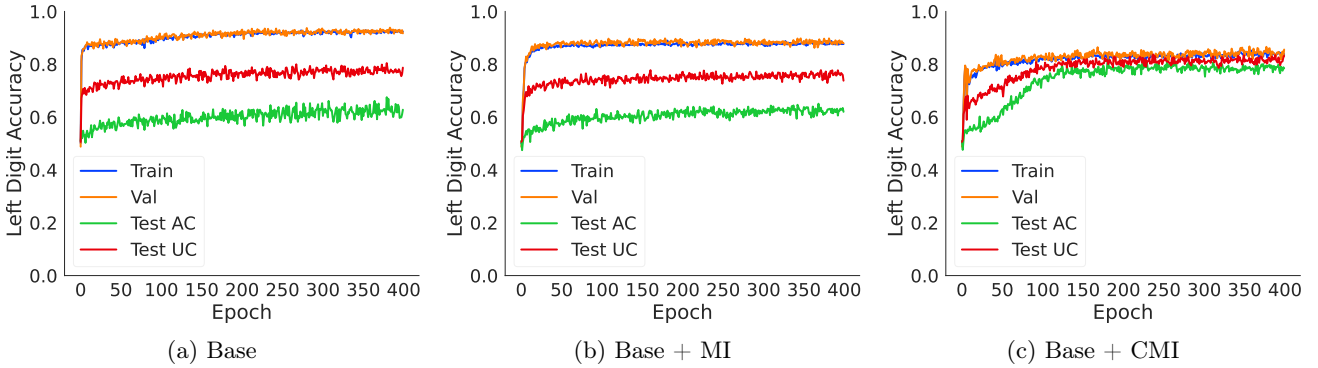


Figure 11: Accuracies for the left digit, under the strongest correlation we consider, $c = 0.9$, at noise level 0.6 (where the noise is parameterized by a factor that has range $[0, 1]$).

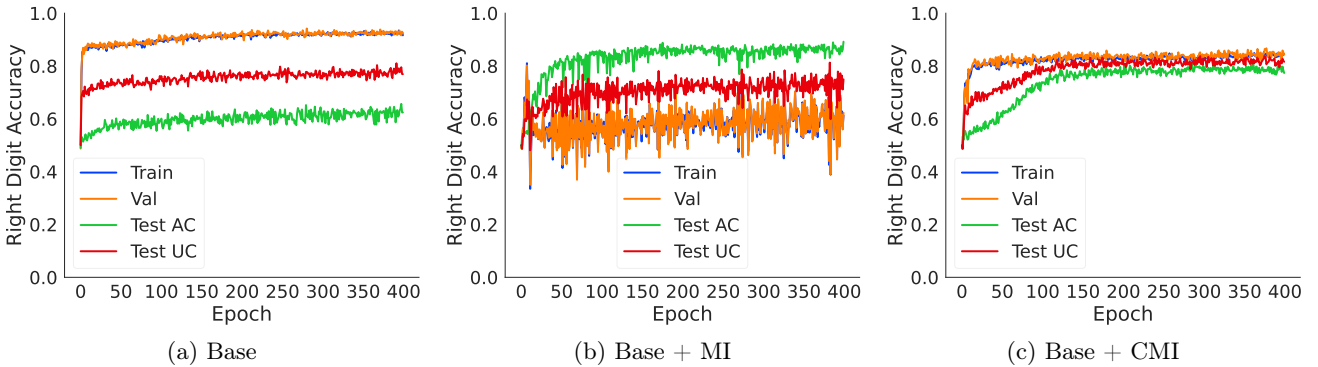


Figure 12: Accuracies for the right digit, under the strongest correlation we consider, $c = 0.9$, at noise level 0.6 (where the noise is parameterized by a factor that has range $[0, 1]$).

B.4 CelebA

For all experiments, we used minibatch size 100, and latent dimension $D = 10$. As the encoder model, we used a three-layer MLP with 50 hidden units per layer and ReLU activations. Similarly to the MNIST setup, we trained for 200 epochs, using Adam to optimize the encoder, linear classifiers, and discriminators. For each method, we performed a grid search over learning rates $\{1e-5, 1e-4, 1e-3\}$ separately for each of the encoder, discriminator(s), and linear classification heads; we selected the best learning rates based on validation accuracy.

Correlated Data Generation. We first pre-processed all images by taking a 128×128 center crop, and then resizing to 64×64 . Pixel values were normalized to the range $[0, 1]$. We used the original training, validation, and test splits provided with the CelebA dataset. In order to enforce arbitrary correlations between specific attributes, we subsampled the data such that we retained the maximum possible number of examples in each of the

Train/Validation/Anticorrelated Test/Uncorrelated Test splits, while satisfying precisely the desired correlation. The validation set has the same correlation as the training set, and Figure 13 shows the number of examples in each of these sets for the strongest correlation we consider, $c = 0.8$. Figures 14, 15, and 16 show the cross-entropy loss and accuracies on each of the factors **Male** and **Smiling** (with training correlation 0.8) over the course of optimization, for each of the methods we compare (classification-only, unconditional disentanglement, and conditional disentanglement). We see that the conditional model substantially outperforms the baselines, with a much smaller gap between validation accuracy and both anti-correlated (AC) and uncorrelated (UC) test accuracies. Figures 17, 18 and 19 show confusion matrices for each method on the correlated validation set, anticorrelated test set, and uncorrelated test set, respectively. Finally, Tables 3 and 4 show the prediction error of the models trained with the different objectives for both the combinations that were common and rare during training. These results shows that some attribute combinations (such as the rare non-smiling male faces) are reliably treated incorrectly.

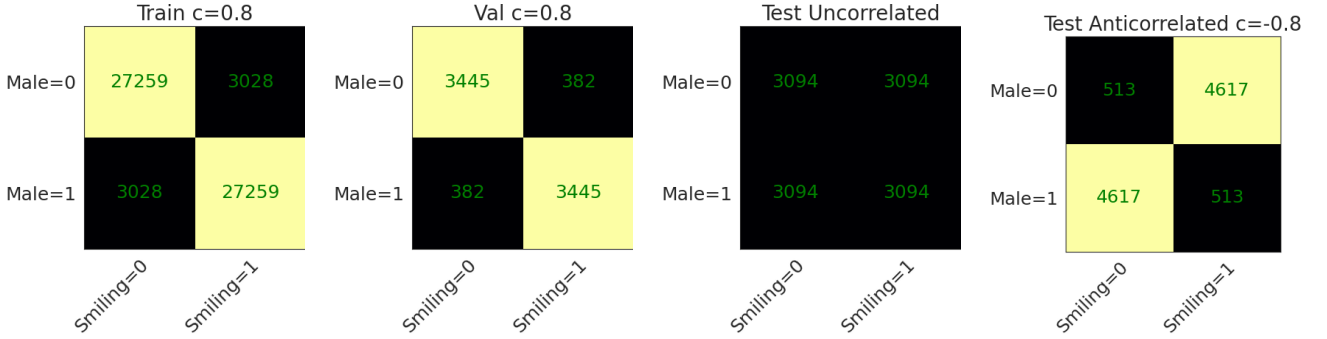


Figure 13: Numbers of examples in the subsampled CelebA datasets for the strongest correlation we consider, $c = 0.8$.

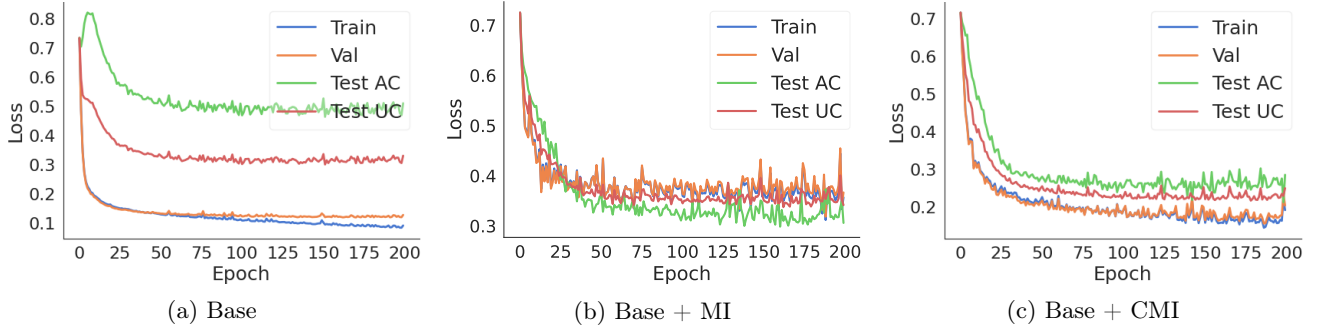


Figure 14: Loss curves for each approach on the **Male-Smiling** CelebA task, under the strongest correlation we consider, $c = 0.8$.

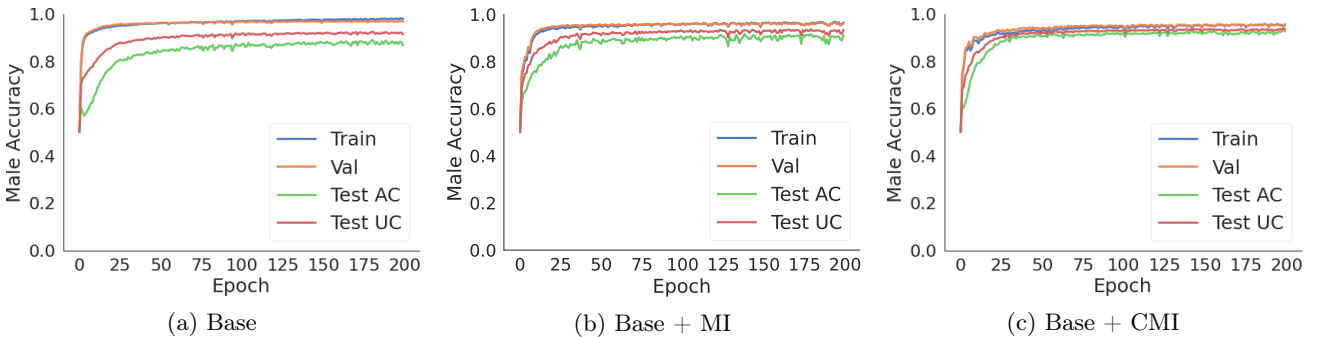


Figure 15: Accuracies on the attribute **Male** for each approach on the **Male-Smiling** CelebA task, under the strongest correlation we consider, $c = 0.8$.

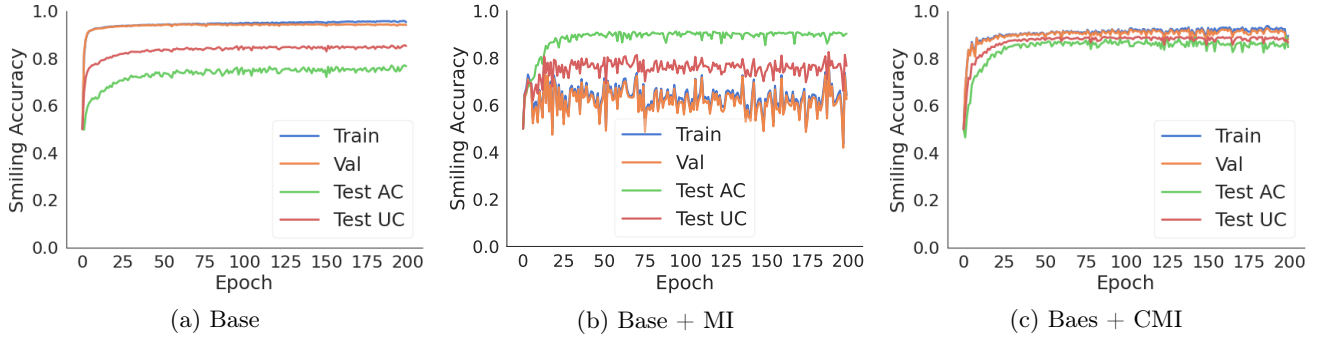


Figure 16: Accuracies on the attribute **Smiling** for each approach on the Male-Smiling CelebA task, under the strongest correlation we consider, $c = 0.8$.

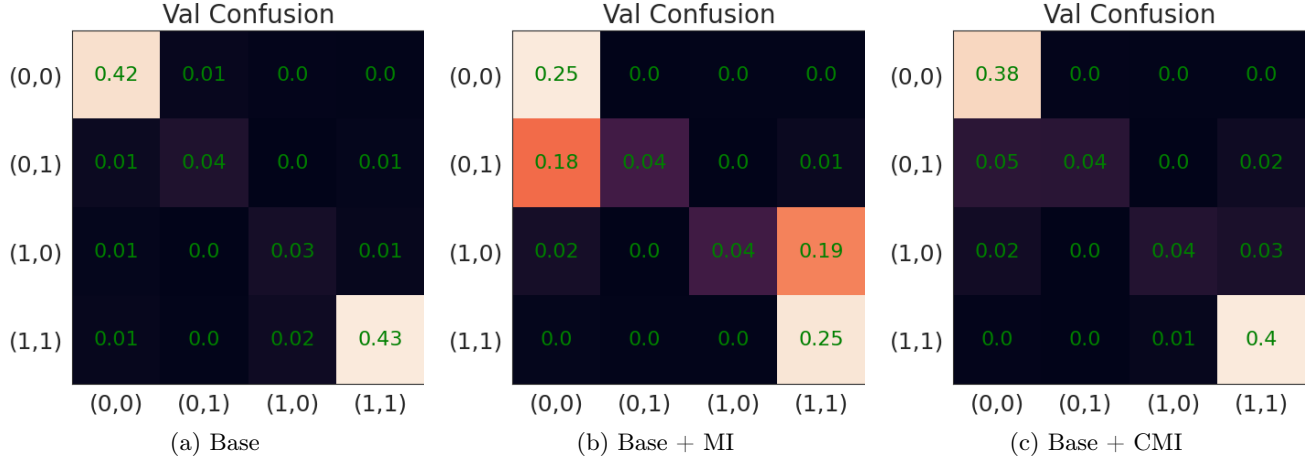


Figure 17: Confusion matrices for each approach on the correlated validation set of the Male-Smiling CelebA task, under the strongest correlation we consider, $c = 0.8$.

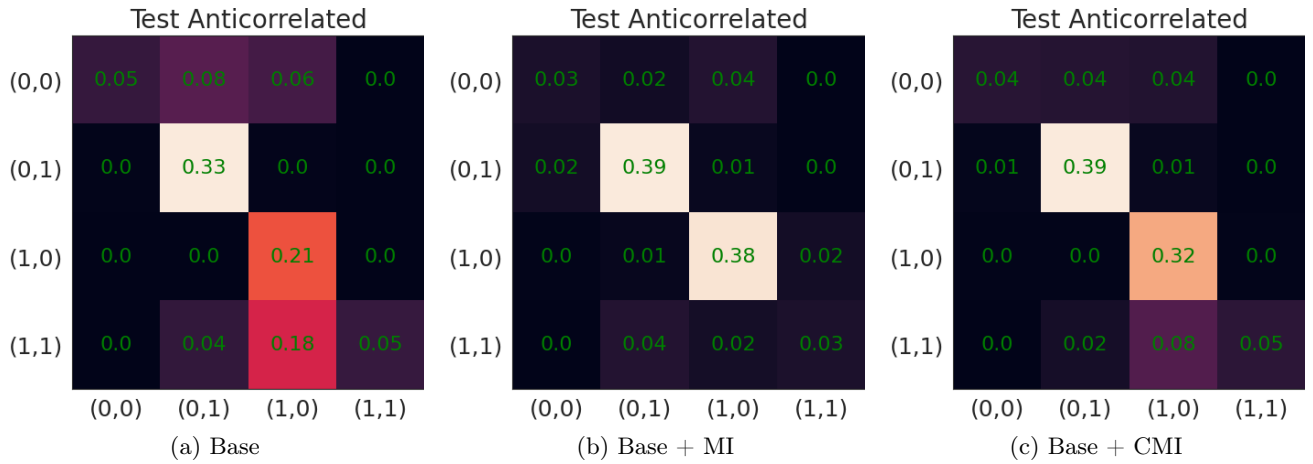


Figure 18: Confusion matrices for each approach on the anti-correlated test set of the Male-Smiling CelebA task, under the strongest correlation we consider, $c = 0.8$.

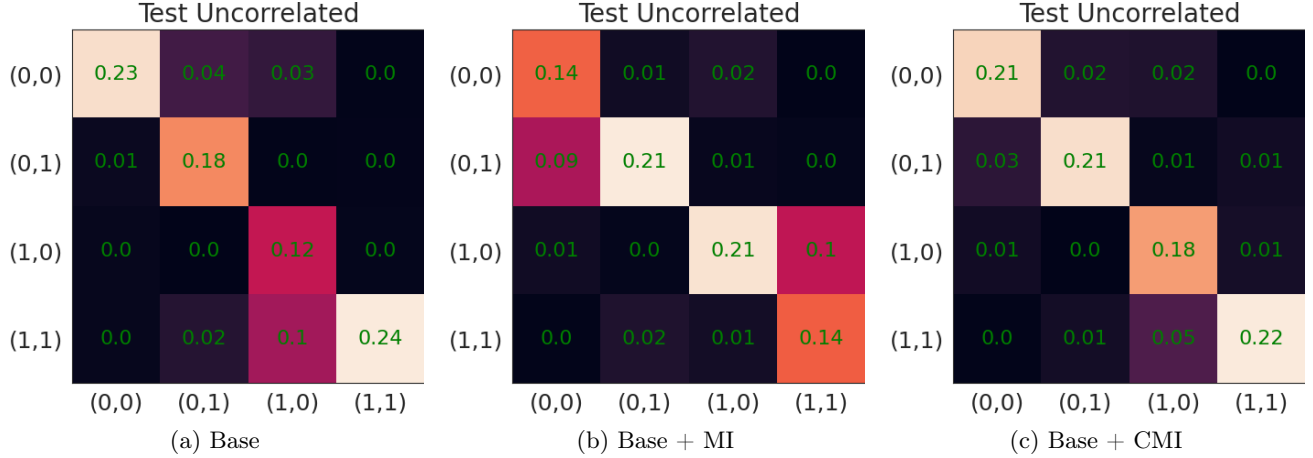


Figure 19: Confusion matrices for each approach on the uncorrelated test set of the Male-Smiling CelebA task, under the strongest correlation we consider, $c = 0.8$.

	Common Combinations		Rare Combinations	
	Female + Non-Smiling	Male + Smiling	Female + Smiling	Male + Non-Smiling
Base	4%	4%	29%	51%
Base + MI	23%	28%	12%	31%
Base + CMI	10%	9%	20%	29%

Table 3: Percentage of incorrect predictions per subgroup for CelebA, evaluated on natural data (e.g., data with naturally-occurring correlations, that has not been subsampled to induce a specific correlation strength), using models trained on correlated data with $c = 0.8$.

	Common Combinations		Rare Combinations	
	Female + Non-Smiling	Male + Smiling	Female + Smiling	Male + Non-Smiling
Base	4%	5%	33%	49%
Base + MI	24%	28%	11%	26%
Base + CMI	9%	9%	19%	25%

Table 4: Percentage of incorrect predictions per subgroup for CelebA, evaluated on validation data ($c = 0.8$), using models trained on correlated data with $c = 0.8$.

B.5 Disentanglement Metrics

We evaluated common disentanglement metrics [57] on uncorrelated test data using models trained on correlated data. We performed this analysis for two of our datasets and found in both cases that *Base+CMI* reached better scores compared to the other objectives for almost all metrics.

Toy Classification: Disentanglement results for the toy classification task with ten attributes are shown in Table 5. We obtained similar results for two and four attributes, which are not reported for brevity.

CelebA: Since the disentanglement metrics require that the factors of variation are each encoded in one-dimensional subspaces, we set latent dimension $D = 2$ for this experiment. In Table 6, we report the average and 68% confidence intervals for five models trained on data with correlation level 0.8.

Metric	Base	Base+MI	Base+CMI
IRS [79] \uparrow	0.377	0.573	0.605
SAP [50] \uparrow	0.118	0.470	0.477
MIG [16] \uparrow	0.179	0.939	0.975
DCI Disentanglement [24] \uparrow	0.413	0.980	0.998
Beta-VAE [33] \uparrow	0.996	1	1
Factor-VAE [45] \uparrow	1	1	1
Gaussian Total Correlation \downarrow	10.073	0.485	0.025
Gaussian Wasserstein Corr \downarrow	12.905	0.373	0.027
Gaussian Wasserstein Corr Norm \downarrow	0.866	0.037	0.002
Mutual Info Score \downarrow	0.975	0.197	0.149

Table 5: **Disentanglement metrics for toy classification with ten attributes.** Metrics are evaluated on the uncorrelated test set. Bold font indicates model with best disentanglement score.

Metric	Base	Base+MI	Base+CMI
IRS \uparrow	0.524 \pm 0.043	0.548 \pm 0.038	0.531 \pm 0.041
SAP \uparrow	0.306 \pm 0.003	0.296 \pm 0.046	0.389 \pm 0.005
MIG \uparrow	0.506 \pm 0.01	0.455 \pm 0.074	0.674 \pm 0.007
DCI Disentanglement \uparrow	0.46 \pm 0.009	0.596 \pm 0.038	0.807 \pm 0.023
Beta-VAE \uparrow	1.0 \pm 0.0	1.0 \pm 0.0	1.0 \pm 0.0
Factor-VAE \uparrow	1.0 \pm 0.0	0.999 \pm 0.003	1.0 \pm 0.0
Gaussian Total Correlation \downarrow	0.222 \pm 0.012	0.056 \pm 0.061	0.011 \pm 0.003
Gaussian Wasserstein Corr \downarrow	0.351 \pm 0.039	0.01 \pm 0.009	0.002 \pm 0.001
Gaussian Wasserstein Corr Norm \downarrow	0.098 \pm 0.005	0.006 \pm 0.004	0.005 \pm 0.001
Mutual Info Score \downarrow	0.302 \pm 0.022	0.111 \pm 0.052	0.042 \pm 0.006

Table 6: **Disentanglement metrics for CelebA.** Metrics are evaluated on the uncorrelated test set. Bold font indicates model with best disentanglement score.

B.6 Weakly Supervised Setting

For the fully supervised CelebA experiment, labels for both attributes were available for all 10260 images. For the weakly supervised setting, we reduced the number of labels to 5130 (50% of the labels of the fully supervised dataset), 2565 (25%), 1026 (10%), or 513 (5%) for each attribute. This implies that some images had both labels, some had only one label and some images had no labels (for example when using 50% of the labels the distinction is as follows: 25% of the images had both labels; 25% had only labels for attribute 1; 25% had only labels for attribute 2; and 25% had no labels). The three objectives can be applied to these weakly supervised settings. For *Base*, the cross-entropy loss for each attribute was computed only for the images that had labels for the corresponding attribute. For *Base+MI* no labels are required for the unconditional shuffling; thus this objective can be applied even for the images without labels. For *Base+CMI*, our method shuffles only images that have the same value for a given attribute. This also works if the labels of the other attribute are missing. We used the same training parameters as for the supervised experiment, except for increasing the number of training epochs (up to 1200 epochs) and adapting the minibatch size to the number of labels. In Figure 5 we report the average and 68% confidence intervals over three runs with different seeds.

C Algorithms

In this section, we provide formal descriptions of the baseline approaches we use. Algorithm 2 describes the classification-only baseline, that trains separate linear classifiers to predict attributes \mathbf{a}_k from the corresponding latent subspaces \mathbf{z}_k . Algorithm 4 describes the unconditional disentanglement baseline, that adversarially minimizes the discrepancy between samples from the joint distribution $p(\mathbf{z}_1, \dots, \mathbf{z}_k)$ and the product of marginals $p(\mathbf{z}_1) \cdots p(\mathbf{z}_k)$.

Algorithm 2 Supervised Learning on Subspaces

```

1: Input:  $\{\phi_1, \dots, \phi_K\}$ , initial parameters for  $K$  linear classifiers  $C_1, \dots, C_K$ 
2: Input:  $\theta$ , initial parameters for the encoder  $F$ 
3: Input:  $\alpha, \beta$  learning rates for training the encoder and linear classifiers
4: while true do
5:    $(\mathbf{x}, \{\mathbf{a}_k\}_{k=1}^K) \sim \mathcal{D}_{\text{Train}}$  ▷ Sample a minibatch of data with attribute labels
6:    $\mathbf{z} \leftarrow F_{\theta}(\mathbf{x})$  ▷ Forward pass through the encoder
7:    $\{\mathbf{z}_k\}_{k=1}^K \leftarrow \text{SplitSubspaces}(\mathbf{z}, k)$  ▷ Partition the latent space into  $k$  subspaces
8:    $L \leftarrow \sum_{k=1}^K L_{\text{cls}}(C_k(\mathbf{z}_k; \phi_k), \mathbf{a}_k)$  ▷ Cross-entropy for each attribute
9:    $\theta \leftarrow \theta - \alpha \nabla_{\theta} L$  ▷ Update encoder parameters
10:   $\phi_k \leftarrow \phi_k - \beta \nabla_{\phi_k} L$  ,  $\forall k \in \{1, \dots, K\}$  ▷ Update classifier parameters
11: end while

```

Algorithm 3 Learning Unconditionally Disentangled Subspaces — Training the Encoder

```

1: Input:  $\{\phi_1, \dots, \phi_K\}$ , initial parameters for  $K$  linear classifiers  $C_1, \dots, C_K$ 
2: Input:  $\theta$ , initial parameters for the encoder  $F$ 
3: Input:  $\alpha, \beta$  learning rates for training the encoder and linear classifiers
4: while true do
5:    $(\mathbf{x}, \{\mathbf{a}_k\}_{k=1}^K) \sim \mathcal{D}_{\text{Train}}$  ▷ Sample a minibatch of data with attribute labels
6:    $\mathbf{z} \leftarrow F_{\theta}(\mathbf{x})$  ▷ Forward pass through the encoder
7:    $\{\mathbf{z}_k\}_{k=1}^K \leftarrow \text{SplitSubspaces}(\mathbf{z}, k)$  ▷ Partition the latent space into  $k$  subspaces
8:    $L \leftarrow \sum_{k=1}^K L_{\text{cls}}(C_k(\mathbf{z}_k; \phi_k), \mathbf{a}_k)$  ▷ Cross-entropy for each attribute
9:    $\mathbf{z}' \sim p(\mathbf{z}_1)p(\mathbf{z}_2) \dots p(\mathbf{z}_k)$  ▷ Samples w/ batchwise-shuffled subspaces
10:   $L \leftarrow L + \log(1 - D_{\omega}(\mathbf{z}')) + \log(D_{\omega}(\mathbf{z}))$  ▷ Add adversarial loss
11:   $\theta \leftarrow \theta - \alpha \nabla_{\theta} L$  ▷ Update encoder parameters
12:   $\phi_k \leftarrow \phi_k - \beta \nabla_{\phi_k} L$  ,  $\forall k \in \{1, \dots, K\}$  ▷ Update classifier parameters
13: end while

```

Algorithm 4 Learning Unconditionally Disentangled Subspaces — Training the Discriminator

```

1: Input:  $\omega$ , initial parameters for the discriminator  $D$ 
2: Input:  $\gamma$ , learning rate for training the discriminator
3: while true do
4:    $(\mathbf{x}, \{\mathbf{a}_k\}_{k=1}^K) \sim \mathcal{D}_{\text{Train}}$  ▷ Sample a minibatch of data with attribute labels
5:    $\mathbf{z} \leftarrow F_{\theta}(\mathbf{x})$  ▷ Forward pass through the encoder
6:    $\{\mathbf{z}_k\}_{k=1}^K \leftarrow \text{SplitSubspaces}(\mathbf{z}, k)$  ▷ Partition the latent space into  $k$  subspaces
7:    $\mathbf{z}' \sim p(\mathbf{z}_1)p(\mathbf{z}_2) \dots p(\mathbf{z}_k)$  ▷ Samples w/ batchwise-shuffled subspaces
8:    $L \leftarrow L + \log(D_{\omega}(\mathbf{z}')) + \log(1 - D_{\omega}(\mathbf{z}))$  ▷ Add adversarial loss
9:    $\omega \leftarrow \omega - \gamma \nabla_{\omega} L$  ▷ Update discriminator parameters
10: end while

```

Algorithm 5 Learning Conditionally Disentangled Subspaces Adversarially – Training the Discriminator

```

1: Input:  $\omega$ , initial parameters for the discriminator  $D$ 
2: Input:  $\gamma$ , learning rate for training the discriminator
3: while true do
4:    $(\mathbf{x}, \{\mathbf{a}_k\}_{k=1}^K) \sim \mathcal{D}_{\text{Train}}$  ▷ Sample a minibatch of data with attribute labels
5:    $\mathbf{z} \leftarrow F_{\theta}(\mathbf{x})$  ▷ Forward pass through the encoder
6:    $\{\mathbf{z}_k\}_{k=1}^K \leftarrow \text{SplitSubspaces}(\mathbf{z}, k)$  ▷ Partition the latent space into  $K$  subspaces
7:    $L \leftarrow 0$  ▷  $L$  will accumulate the losses over all subspaces
8:   for  $k \in \{1, \dots, K\}$  do
9:      $\mathbf{z}' \sim p(\mathbf{z}_1, \dots, \mathbf{z}_K \mid \mathbf{a}_k)$  ▷ Samples from the joint distribution
10:     $\mathbf{z}'' \sim p(\mathbf{z}_k \mid \mathbf{a}_k)p(\mathbf{z}_{-k} \mid \mathbf{a}_k)$  ▷ Samples w/ batchwise-shuffled subspaces
11:     $L \leftarrow L + \log(D_{\omega}(\mathbf{z}'')) + \log(1 - D_{\omega}(\mathbf{z}'))$  ▷ Add adversarial loss
12:   end for
13:    $\omega \leftarrow \omega - \gamma \nabla_{\omega} L$  ▷ Update discriminator parameters
14: end while

```

D Proof of Proposition 3.1

Proposition 3.1 *If $I(s_1; s_2) > 0$, then enforcing $I(z_1; z_2) = 0$ means that $I(z_k; s_k) < H(s_k)$ for at least one k .*

Proof. Assume that $I(s_1; s_2) > 0$ and at the same time $I(z_k; s_k) = H(s_k)$ (i.e., we are proving by contradiction). Since $I(z_1; s_1) = H(s_1)$, we have $H(s_1 | z_1) = 0$ and with $H(s_1 | z_1) = H(s_1 | z_1, s_2) + I(s_1; s_2 | z_1)$ (both non-negative), it follows that $H(s_1 | z_1, s_2) = I(s_1; s_2 | z_1) = 0$. Since for the interaction information, by definition $I(s_1; s_2; z_1) = I(s_1; s_2) - I(s_1; s_2 | z_1)$, and $I(s_1; s_2 | z_1) = 0$, we have $I(s_1; s_2; z_1) = I(s_1; s_2) > 0$. Since we also assume $H(s_2 | z_2) = 0$, we also have $I(s_1; s_2; z_2) = I(s_1; s_2) > 0$.

We can use this to compute the fourth order interaction information $I(s_1; s_2; z_1; z_2)$. By definition, we have $I(s_1; s_2; z_1; z_2) = I(s_1; s_2; z_1) - I(s_1; s_2; z_1 | z_2)$. We just showed that $I(s_1; s_2; z_1) = I(s_1; s_2)$, and therefore we have $I(s_1; s_2; z_1 | z_2) = I(s_1; s_2 | z_2)$. Together it follows that:

$$I(s_1; s_2; z_1; z_2) = I(s_1; s_2; z_1) - I(s_1; s_2; z_1 | z_2) \quad (7)$$

$$= I(s_1; s_2) - I(s_1; s_2 | z_2) \quad (8)$$

$$= I(s_1; s_2; z_2) \quad (9)$$

$$= I(s_1; s_2) > 0 \quad (10)$$

On the other hand, we know that $0 = H(s_1 | z_1) = H(s_1 | z_1; z_2) + I(s_1, z_2 | z_1)$ and therefore $I(s_1, z_2 | z_1) = 0$. Therefore, the interaction information $I(s_1; z_2; z_1) = I(s_1; z_2) - I(s_1; z_2 | z_1) = I(s_1; z_2) \geq 0$. At the same time, we assumed that $I(z_1; z_2) = 0$ and hence $I(z_1; z_2; s_1) + I(z_1; z_2 | s_1) = 0$, which shows that $I(z_1; z_2; s_1) \leq 0$. Together, we see that $I(z_1; z_2; s_1) = I(s_1; z_2) = 0$.

Now we can decompose $I(s_1; s_2; z_1; z_2)$ in a different way: $I(s_1; s_2; z_1; z_2) = I(s_1; z_1; z_2) - I(s_1; z_1; z_2 | s_2)$. We know that $I(s_1; z_1; z_2) = I(s_1; z_2)$ and therefore $I(s_1; z_1; z_2 | s_2) = I(s_1; z_2 | s_2) > 0$ and that $I(s_1; z_1; z_2) = 0$. Therefore, it follows that:

$$I(s_1; s_2; z_1; z_2) = I(s_1; z_1; z_2) - I(s_1; z_1; z_2 | s_2) \quad (11)$$

$$= 0 - I(s_1; z_2 | s_2) \quad (12)$$

$$\leq 0 \quad (13)$$

which is a contradiction with $I(s_1; s_2; z_1; z_2) = I(s_1; s_2) > 0$. Therefore, if $I(s_1; s_2) > 0$ and $I(z_1; z_2) = 0$, it must hold that $I(z_k; s_k) < H(s_k)$ for at least one k , which we wanted to show. \square